Title:

Analytical study on wave power extraction from a hybrid wave energy converter

Author names and affiliations:

Siming Zheng

State Key Laboratory of Hydroscience and Engineering, Tsinghua University, Beijing 100084, China

E-mail address: zhengsm@tsinghua.edu.cn

Yongliang Zhang

State Key Laboratory of Hydroscience and Engineering, Tsinghua University, Beijing 100084, China

E-mail address: yongliangzhang@tsinghua.edu.cn

Corresponding author:

Yongliang Zhang

State Key Laboratory of Hydroscience and Engineering, Tsinghua University, Beijing 100084, China

Tel.: + 86 10 62797802

E-mail address: yongliangzhang@tsinghua.edu.cn

Accepted 8 July 2018

https://doi.org/10.1016/j.oceaneng.2018.07.021

Analytical study on wave power extraction from a hybrid wave energy converter

Abstract: In this paper, a hybrid wave energy converter (WEC) is proposed, consisting of a fixed inverted flume with long length and a bottom hole, and a long floating cube hinged with the flume. The inverted flume and the long floating cube works as an oscillating water column (OWC) and a rotational float, respectively, to capture power from incident waves. To study the performance of this hybrid WEC, analytical solution of the wave diffraction/radiation problems, considering the hydrodynamic interaction between the OWC and the float, is derived based on linear potential flow theory and eigen-function expansion matching method in the two-dimensional Cartesian coordinate systems. The corresponding hydrodynamic coefficients, such as wave excitation forces, added mass and wave radiation damping, are also obtained, which can be further used in evaluation of the maximum theoretical power absorption of the hybrid WEC. Results are compared with a parallel study of an isolated OWC and an isolated float. Additionally, analytical study on power capture capability of the device for various geometrical parameters is then carried out.

Keywords: Linear potential flow theory, Analytical model, Wave power extraction, Oscillating Water Column, Hinged float

1. Introduction

Oscillating water column (OWC) has been recognized as one of the most effective concepts of wave energy conversion, which mainly consists of a partially submerged rigid chamber and exploits wave power by driving an air turbine using the oscillating motion of the inner free water surface (Heath, 2012; Malara and Arena, 2013; Deng et al., 2014; He and Huang, 2017; Chen et al., 2017). To understand and improve wave power extraction by OWC devices, experimental, numerical, and analytical methods have been widely employed and many different design of OWC devices have been proposed as well.

Experimental tests present a straightforward way to study the performance of OWC devices. For the case where the OWC is very long in the horizontal co-ordinate compared to the wave length, wave diffraction and radiation from the OWC can be concerned with a two-dimensional problem. Sarmento (1992) carried out wave flume experiments on two-dimensional OWC devices and found a good agreement between the experimental data and the prediction values from linear theory. Morris-Thomas et al. (2007) experimentally studied a shore based oscillating OWC device, and found that the increase in front wall submergence reduced the power capture efficiency in short waves. He et al. (2013, 2017) considered the integration of OWC devices with a floating breakwater, which was experimentally found to be a promising way to widen the frequency range for power extraction. Due to the constraints of laboratory facilities, funding and time in conducting experimental studies of OWC devices, numerical and analytical methods were preferred by many researchers.

Numerical studies on OWC devices are commonly performed by using BEM (Boundary Element Method) models and RANS (Reynolds-Averaged Navier-Stokes equations) models, which are based on potential flow theory and viscous fluid theory, respectively. Sheng et al. (2014) used an imaginary “piston” to replace part of the water at the internal water surface in the OWC chamber and solved the hydrodynamic problems from the device itself and the imaginary “piston” by using a commercial BEM model. Appropriate representation of the “imaginary” piston was found very

important, when the hydrodynamic parameters were to be transformed from frequency-domain to time domain for a further analysis. Rezanejad et al. (2013, 2015) adopted BEM method to analyse the efficiency of a two-dimensional nearshore multiple OWC devices placed over flat bottom and stepped bottom, respectively. Ning et al. (2015, 2017) applied a fully nonlinear numerical wave flume based on higher-order BEM in simulating of both one-chamber and dual-chamber OWC devices. Numerical results indicated that the surface elevations in the two sub-chambers are strongly dependent on the wave conditions. Compared with BEM models, the RANS models are capable to handle problems with very strong nonlinearity induced by turbulence, viscous, vortex shedding and wave breaking. Elhanafi et al. (2016, 2017) used a fully nonlinear 2D RANS model to carry out analysis of onshore and offshore OWC devices, respectively. Frequency response of the overall hydrodynamic efficiency showed a single-peaked curve and it was revealed that increase of the submergence of lips was beneficial to the energy extraction in long waves, whereas went against power absorption for short waves. Other numerical investigations on OWC devices with implementation of RANS models can be found in Zhang et al. (2012), López et al. (2014, 2016), Iturrioz et al. (2015). However, as the RANS model utilized in the above-mentioned numerical simulations normally requires a much more computational power, its employment is limited to a certain extent in some ways.

For the OWCs in regular shapes, the analytical method, which is generally based on potential flow theory and eigen-function expansions, can be a good alternative option, especially in their pre-feasibility study and even their feasibility study, and can be used to provide insights and important information rapidly at relatively low costs.

As early as 1980s, Evans (1982) presented theoretical results of wave-power absorption by a two-dimensional system of uniform oscillatory surface pressure distributions based on the linearized hydrodynamic theory. Later, Falnes and McIver (1985) applied analytical method to study the power absorption by an OWC, which is composed of two vertical barriers with unequal length, oscillating in the surge mode. It was shown that all of the incident wave power can be captured by the system with optimum values of the complex oscillation amplitudes. Sarmento and Falcão (1985) developed an analytical analysis for an OWC device in which the immersed part of the OWC was assumed of shallow draught. Evans and Porter (1995) described an accurate model using matched eigen-function expansions and a Galerkin method to compute the hydrodynamic coefficients associated with an OWC device consisting of a thin vertical surface-piercing barrier next to a vertical wall. This method has been widely used in solving the hydrodynamic problems of the OWC based on thin barrier assumption. It was found that the OWC with a larger chamber width had a smaller wave frequency at which resonance occurs. Rezanejad et al. (2013) studied the performance of a dual-chamber OWC device which consists of two vertical thin barriers in front of a vertical wall. It was revealed that the draft of the outside chamber was a dominant parameter determining the basic resonance frequency of power extraction. Later, the dual-chamber OWC with vertical thin barriers placed over stepped bottom was also analysed (Rezanejad et al., 2015). Noad and Porter (2017) considered a simplified model of a shallow-draughted multiple-chamber OWC which is comprised of a series of open bottomed chambers each enclosing an internal free surface. It was identified that variations in chamber sizing were advantageous, with larger chambers positioned to the aft, not only dividing the power capture more evenly between the chambers, but also leading to a broader-banded response. As another development of the simple OWC, the U-OWC device utilizing a small vertical U-duct for connecting the air pocket to the open wave field was introduced and its performance was analytically investigated by Boccotti (2007) and Malara and Arena (2013). While due to either "thin barrier" or "shallow draught barrier" assumptions, the analytical models proposed so far are not valid in dealing with a more common situation, where the thickness and draught of the OWC chamber cannot be ignored. Although Zheng and Zhang (2016) have recently developed an analytical model for diffraction and radiation problems of multiple floats, in which any two adjacent floats might be seen as the fore and aft walls of OWC with arbitrary thickness, the

radiation problem due to pressure oscillation inside the OWC chamber has not been taken into account.

This paper extends the previously mentioned traditional offshore OWC concept, discussed by Elhanafi et al. (2017), by considering a long oscillating floating cube hinged onto the OWC. The aim is to enhance the performance of overall wave energy absorption. Apart from harnessing power by the air turbine at the top of the OWC, rotation of the float (the long oscillating floating cube) relative to the OWC can also be adopted to drive a cylinder installed between the OWC and float, extracting wave power. Therefore, the device might be named as a hybrid wave energy converter (WEC). On the one hand, due to the physical connection of the oscillating float onto the OWC, no mooring system is required for the float and the costs of construction could be reduced. On the other hand, it is believed that, with an optimized dimension, power extraction of the hybrid WEC can be obviously improved for a large range of wave frequencies due to the hydrodynamic interaction between the OWC and oscillating float. To study the hydrodynamic performance of the hybrid WEC, the previously mentioned analytical model for the diffraction and radiation problem from multiple floats, discussed by Zheng and Zhang (2016) is extended by considering the radiation due to pressure oscillation between two adjacent floats, and then employed to carry out a geometric parametric study of the hybrid WEC. Results are compared with a parallel study of an isolated OWC and an isolated float.

The rest of the paper is organized as follows. Section 2 describes the analytical model used in the hydrodynamic simulations. Section 3 presents the validation of the analytical model. Results and discussions are provided in Section 4. Conclusions are summarized in Section 5.

2. Analytical model

2.1. Problem description

The hybrid WEC proposed is mainly composed of a fixed OWC chamber and a float, as shown in Fig. 1. The float is connected to the fore wall of the OWC through a rigid arm. As ocean waves pass through the hybrid WEC, the OWC can be used to drive an air turbine and a motor installed at the top of the OWC chamber to capture wave power. Additionally, the wave-induced rotation of the float around the hinge can be employed to drive a hydraulic cylinder installed between the rigid arm and the OWC to exploit wave power as well.

It is assumed that the monochromatic incident waves of small amplitude A and frequency ω propagate perpendicularly to the WEC and the length of the hybrid WEC along the crest line of these incident waves is much larger than wave length. Therefore, wave diffraction/radiation problems of this WEC can be treated as two-dimensional ones. As given in Fig. 1, a Cartesian coordinate (x, z) system with its original point O located at the point of intersection of the mean water surface and the front wall of the float is used to formulate the hydrodynamic problem of the hybrid WEC, in which x and z denote the incident wave propagation and the upward direction, respectively. The width of the float, the thickness of the fore wall and aft wall of OWC chamber are denoted as a_1, a_2 and a_3, respectively. The draft of the float, the submergence of the fore wall and aft wall of OWC chamber are denoted as d_1, d_2 and d_3, respectively. a represents the water column width inside the OWC chamber; d denotes the height of the hinge relative to the mean water surface; D represents the distance between the float center and the fore wall of OWC. The water area is considered with a constant depth of h. As shown in Fig.1, if we choose the hinge

point as a reference point of the float motion, the floater has only one degree of freedom, i.e. pitch rotation relative to the hinge point. In such situation, the excitation pitch moment and the hydrodynamic coefficients in rotation mode of the float are strongly dependent on the height of the hinge relative to the mean water surface, i.e. d. In this paper, the center of gravity of the float (x_0, z_0) is used as the reference point to calculate the motion response of the float. Hence surge, heave and pitch modes should all be considered in solving wave diffraction and radiation problems. The mechanical relation between the surge/heave and pitch modes induced by the hinge constraint can be further taken into account in evaluating motion response of the WEC without resolving hydrodynamic problem for different d.

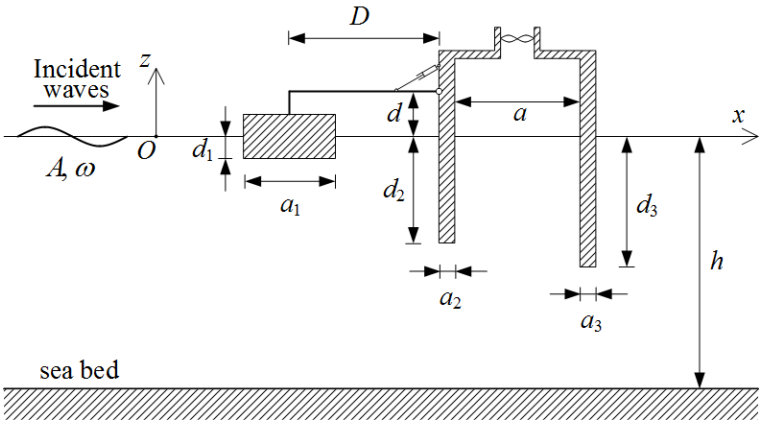

Fig. 1. Definition sketch of the hybrid WEC

In common with the assumptions that have been adopted by Zheng and Zhang (2016), in this paper, the fluid is considered isotropic and incompressible inviscid, the time-harmonic flow is irrotational, and the deformation of both float and OWC chamber are neglected.

With the employment of linear potential flow theory, the fluid motion can be expressed by the velocity potential $\varphi = \mathrm{Re}\left[\Phi(x,z)\mathrm{e}^{-\mathrm{i}\omega t}\right]$, where Φ is a complex spatial velocity potential satisfying the Laplace equation; i is the imaginary unit and t is the time.

Φ can be decomposed into an incident wave spatial potential Φ_I, a diffracted wave spatial potential Φ_D and four radiated wave spatial potential $\Phi_\mathrm{R}^{(L)}$:

$$\Phi = \Phi_\mathrm{I} + \Phi_\mathrm{D} + \sum_{L=1}^{3} \dot{A}_L \Phi_\mathrm{R}^{(L)} + p\Phi_\mathrm{R}^{(4)}, \tag{1}$$

where $\dot{A}_L$ is the complex amplitude of the float velocity oscillation in mode L (L=1, 2, 3, which represent surge, heave and pitch, respectively); $\Phi_\mathrm{R}^{(L)}$(L=1, 2, 3) is the spatial velocity potential due to unit amplitude velocity oscillation of the float in mode L; p is the complex air pressure

amplitude inside the OWC chamber; $\Phi_{\mathrm{R}}^{(4)}$ is the spatial velocity potential due to unit air pressure oscillation inside the OWC chamber.

Expression of Φ_{I}, the dominate equation and the boundary conditions that Φ_{D} and $\Phi_{\mathrm{R}}^{(L)}$(L=1, 2, 3) should satisfy can all be found in our previous paper (Zheng and Zhang, 2016). Compared with $\Phi_{\mathrm{R}}^{(L)}$(L=1, 2, 3), due to the existence of air pressure oscillation inside the OWC chamber, the only different boundary condition for $\Phi_{\mathrm{R}}^{(4)}$ happens on the free water surface in the OWC chamber, where $\Phi_{\mathrm{R}}^{(4)}$ should satisfy

$$\frac{\partial \Phi_{\mathrm{R}}^{(4)}}{\partial z}-\frac{\omega^2}{g}\Phi_{\mathrm{R}}^{(4)}=\frac{\mathrm{i}\omega}{\rho g}, \tag{2}$$

in which ρ is the water density and g is the gravity acceleration.

2.2. Formulation of the wave diffraction/radiation problem

To solve the wave diffraction and radiation problems, the fluid domain is divided into 7 subdomains denoted as Ω_j (j=1, 2, …, 7) as shown in Fig. 2.

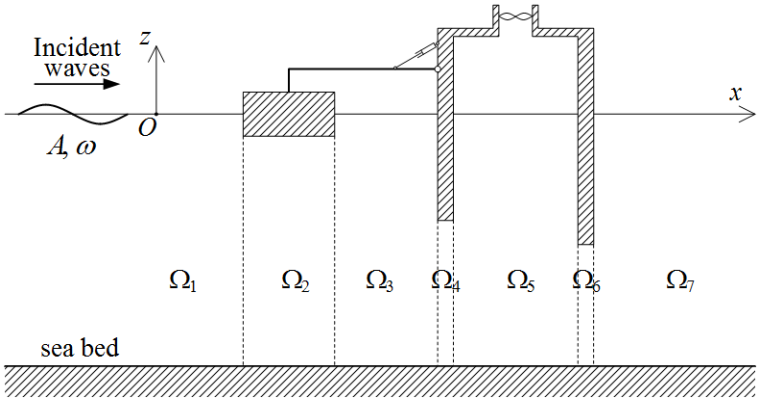

Fig. 2 Sketch of the subdomains of water domain

Utilizing the method of separation of variables, the analytical expressions for unknown diffracted/radiated spatial potential in each subdomain can be obtained as follows (Zheng and Zhang, 2016; Falnes, 2002):

Wave diffraction problem

In regions 1, 2m+1, 2m and 7, the diffracted potentials may be expressed, respectively, as follows:

$$\Phi_{\mathrm{D},1}=\sum_{j=1}^{\infty}A_{1,j}^{\mathrm{D}}\mathrm{e}^{\lambda_j x}Z_j(z)\ \text{ in }\Omega_1. \tag{3}$$

For m=1, 2,

$$\Phi_{\mathrm{D},2m+1}=\sum_{j=1}^{\infty}\left(A_{2m+1,j}^{\mathrm{D}}\mathrm{e}^{\lambda_j x}+B_{2m+1,j}^{\mathrm{D}}\mathrm{e}^{-\lambda_j x}\right)Z_j\left(z\right)\ \text{ in }\Omega_{2m+1}. \tag{4}$$

For m=1, 2, 3,

$$\Phi_{\mathrm{D},2m}=-\Phi_{\mathrm{I}}+A_{2m,1}^{\mathrm{D}}x+B_{2m,1}^{\mathrm{D}}+\sum_{j=2}^{\infty}\left(A_{2m,j}^{\mathrm{D}}\mathrm{e}^{\beta_{m,j}x}+B_{2m,j}^{\mathrm{D}}\mathrm{e}^{-\beta_{m,j}x}\right)\cos\left[\beta_{m,j}\left(z+h\right)\right]\ \text{ in }\Omega_{2m}. \tag{5}$$

$$\Phi_{\mathrm{D},7}=\sum_{j=1}^{\infty}A_{7,j}^{\mathrm{D}}\mathrm{e}^{-\lambda_j x}Z_j\left(z\right)\ \text{ in }\Omega_{7}. \tag{6}$$

$A_{1,j}^{\mathrm{D}}$, $A_{2m+1,j}^{\mathrm{D}}$, $B_{2m+1,j}^{\mathrm{D}}$, $A_{2m,j}^{\mathrm{D}}$, $B_{2m,j}^{\mathrm{D}}$ and $A_{7,j}^{\mathrm{D}}$ as given in Eqs. (3)~(6) are unknown coefficients to be determined; Eq. (4) represents a general wave solution for the velocity potential in a uniform fluid of constant depth (Falnes, 2002); $\beta_{m,j}$ and λ_j are the eigenvalues of the j-th wave modes in subdomain 2m, and subdomains 1 and 2, respectively, given as:

$$\lambda_1=-\mathrm{i}k,\ j=1, \tag{7}$$

$$\omega^2=-\lambda_j g\tan\left(\lambda_j h\right),\ j=2, 3, 4, \ldots, \tag{8}$$

$$\beta_{m,j}=\frac{\left(j-1\right)\pi}{h-d_m},\ j=2, 3, 4, \ldots, \tag{9}$$

$$Z_j\left(z\right)=N_j^{-0.5}\cos\left[\lambda_j\left(h+z\right)\right],\ \ N_j=\frac{1}{2}\left[1+\frac{\sin\left(2\lambda_j h\right)}{2\lambda_j h}\right], \tag{10}$$

in which k is the wave number satisfying $\omega^2=gk\tanh\left(kh\right)$.

Wave radiation problem

In regions 1, 2m+1, 2m and 7, the radiated potentials can be expressed, respectively, as follows:

$$\Phi_{\mathrm{R},1}^{(L)}=\sum_{j=1}^{\infty}A_{1,j}^{(L)}\mathrm{e}^{\lambda_j x}Z_j\left(z\right)\ \text{ in }\Omega_{1}. \tag{11}$$

For m=1,2,

$$\Phi_{\mathrm{R},2m+1}^{(L)}=\sum_{j=1}^{\infty}\left(A_{2m+1,j}^{(L)}\mathrm{e}^{\lambda_j x}+B_{2m+1,j}^{(L)}\mathrm{e}^{-\lambda_j x}\right)Z_j\left(z\right)-\frac{\mathrm{i}\delta_{L,4}\delta_{m,2}}{\rho\omega}\ \text{ in }\Omega_{2m+1}. \tag{12}$$

For m=1, 2, 3,

$$\Phi_{\mathrm{R},2m}^{(L)}=\Phi_{\mathrm{R},2m}^{\mathrm{p},L}+A_{2m,1}^{(L)}x+B_{2m,1}^{(L)}+\sum_{j=2}^{\infty}\left(A_{2m,j}^{(L)}\mathrm{e}^{\beta_{m,j}x}+B_{2m,j}^{(L)}\mathrm{e}^{-\beta_{m,j}x}\right)\cos\left[\beta_{m,j}\left(z+h\right)\right]\ \text{ in }\ \Omega_{2m}\ .(13)$$

$$\Phi_{\mathrm{R},7}^{(L)}=\sum_{j=1}^{\infty}A_{7,j}^{(L)}\mathrm{e}^{-\lambda_j x}Z_j\left(z\right)\ \text{ in }\ \Omega_7\ . \tag{14}$$

In Eqs.(7)~(10), $A_{1,j}^{(L)}$, $A_{2m+1,j}^{(L)}$, $B_{2m+1,j}^{(L)}$, $A_{2m,j}^{(L)}$, $B_{2m,j}^{(L)}$ and $A_{7,j}^{(L)}$ are unknown coefficients to be determined; $\delta_{i,j}$ denotes the Kronecker delta, and $\Phi_{\mathrm{R},2m}^{\mathrm{p},L}$ represents a special solution of $\Phi_{\mathrm{R},2m}^{(L)}$ expressed as

$$\Phi_{\mathrm{R},2m}^{\mathrm{p},L}=\delta_{m,1}\left[\frac{\left(z+h\right)^2-x^2}{2\left(h-d_m\right)}\delta_{2,L}-\frac{\left(z+h\right)^2\left(x-x_0\right)-\frac{1}{3}\left(x-x_0\right)^3}{2\left(h-d_m\right)}\delta_{3,L}\right]. \tag{15}$$

2.3. Solution to diffracted/radiated potentials

At either the interface between two adjacent subdomains or the fluid-structure interface, the motions of the structures and fluids is fully coupled by pressures or/and velocities normal to the interfaces. The continuity conditions at these interfaces for Φ_{D} has been previously given in Zheng and Zhang (2016). To shorten the paper length, here only the continuity conditions for $\Phi_{\mathrm{R}}^{(L)}$(L=1, 2, 3, 4) are presented as follows:

$$\frac{\partial\Phi_{\mathrm{R},2m-1}^{(L)}}{\partial x}=\begin{cases}\delta_{m,1}\left[\delta_{1,L}+\left(z-z_0\right)\delta_{3,L}\right] & \left(x=x_{\mathrm{L},m},\quad -d_m<z<0\right)\\ \dfrac{\partial\Phi_{\mathrm{R},2m}^{(L)}}{\partial x} & \left(x=x_{\mathrm{L},m},\quad -h<z<-d_m\right)\end{cases}, \tag{16}$$

$$\frac{\partial\Phi_{\mathrm{R},2m+1}^{(L)}}{\partial x}=\begin{cases}\delta_{m,1}\left[\delta_{1,L}+\left(z-z_0\right)\delta_{3,L}\right] & \left(x=x_{\mathrm{R},m},\quad -d_m<z<0\right)\\ \dfrac{\partial\Phi_{\mathrm{R},2m}^{(L)}}{\partial x} & \left(x=x_{\mathrm{R},m},\quad -h<z<-d_m\right)\end{cases}, \tag{17}$$

$$\Phi_{\mathrm{R},2m-1}^{(L)}=\Phi_{\mathrm{R},2m}^{(L)}\qquad\left(x=x_{\mathrm{L},m},\quad -h<z<-d_m\right), \tag{18}$$

$$\Phi_{\mathrm{R},2m}^{(L)}=\Phi_{\mathrm{R},2m+1}^{(L)}\qquad\left(x=x_{\mathrm{R},m},\quad -h<z<-d_m\right), \tag{19}$$

where $x_{\mathrm{L},m}$ and $x_{\mathrm{R},m}$ represent the horizontal positions of the left and right edges of subdomain Ω_{2m}, respectively.

Upon substituting Eqs (3–6) for Φ_{D} in different subdomains into the continuity conditions for wave diffraction and Eqs.(11-14) for $\Phi_{\mathrm{R}}^{(L)}$ in different subdomains into Eqs.(16-19), utilizing the orthogonality relations of the integration of eigen-functions over the vertical dimension (Zheng and Zhang, 2016) and taking the first M terms in the infinite series, a linear system of $12M$ complex equations for either Φ_{D} or $\Phi_{\mathrm{R}}^{(L)}$ with the same number of unknown coefficients are obtained. The unknown coefficients can be easily evaluated by solving a $12M$-order linear matrix equation.

2.4. Hydrodynamic coefficients due to wave diffraction/radiation

2.4.1 Direct Method (DM) for solving hydrodynamic coefficients

wave diffraction

For fixed structures, the hydrodynamic forces acting on them called wave excitation forces are induced by both the undisturbed incident wave and the diffracted wave. The wave excitation force loading on the float in mode L (L=1, 2, 3) can be written as $\mathrm{Re}\left(F_{\mathrm{e}}^{(L)}\mathrm{e}^{-\mathrm{i}\omega t}\right)$, in which from the view of the definition of "wave excitation force", $F_{\mathrm{e}}^{(L)}$ is expressed as

$$F_{\mathrm{e}}^{(L)} = -\mathrm{i}\omega\rho\int_{S_1}\left(\Phi_{\mathrm{I}}+\Phi_{\mathrm{D}}\right)n_L\mathrm{d}s\,, \tag{20}$$

where S_1 is the wetted surface of the float; n_L is the component in mode L of the generalized normal vector.

Similarly, the upward flux at the water surface inside the OWC chamber due to the contributions of undisturbed incident wave and the diffracted wave, so-called the excitation volume flow, can be written as

$$F_{\mathrm{e}}^{(4)} = \int_{x_{\mathrm{R},2}}^{x_{\mathrm{L},3}}\frac{\partial\left(\Phi_{\mathrm{I}}+\Phi_{\mathrm{D}}\right)}{\partial z}\Big|_{z=0}\mathrm{d}x\,. \tag{21}$$

wave radiation

Radiation force acting on the float in mode i (i=1, 2, 3) can be treated as one that is induced by the oscillations of both the float and the OWC written as $\mathrm{Re}\left(F_{\mathrm{R}}^{(i)}\mathrm{e}^{-\mathrm{i}\omega t}\right)$, in which

$$\begin{aligned} F_{\mathrm{R}}^{(i)} &= -\mathrm{i}\omega\rho\int_{S_1}\left(\sum_{L=1}^{3}\dot{A}_L\Phi_{\mathrm{R}}^{(L)}+p\Phi_{\mathrm{R}}^{(4)}\right)n_i\mathrm{d}s \\ &= -\mathrm{i}\omega\rho\int_{S_1}\sum_{L=1}^{4}\dot{A}_L\Phi_{\mathrm{R}}^{(L)}n_i\mathrm{d}s = \sum_{L=1}^{4}\dot{A}_L\left(\mathrm{i}\omega a_{i,L}-c_{i,L}\right) \end{aligned}, \tag{22}$$

where $\dot{A}_4 = p$, $a_{i,L} = -\rho\int_{S_1}\mathrm{Re}\left(\Phi_{\mathrm{R}}^{(L)}\right)n_i\mathrm{d}s$, and $c_{i,L} = -\rho\omega\int_{S_1}\mathrm{Im}\left(\Phi_{\mathrm{R}}^{(L)}\right)n_i\mathrm{d}s$.

Similarly, the upward flux at the water surface inside the OWC chamber due to the radiated waves induced by the oscillations of both the float and the OWC can be written as

$$\begin{aligned} F_{\mathrm{R}}^{(4)} &= \int_{x_{\mathrm{R},2}}^{x_{\mathrm{L},3}} \frac{\partial \sum_{L=1}^{4} \dot{A}_L \Phi_{\mathrm{R}}^{(L)}}{\partial z}\Big|_{z=0} \mathrm{d}x \\ &= \frac{\omega^2}{g} \sum_{L=1}^{4} \dot{A}_L \sum_{j=1}^{\infty} \int_{x_{\mathrm{R},2}}^{x_{\mathrm{L},3}} \left(A_{5,j}^{(L)} \mathrm{e}^{\lambda_j x} + B_{5,j}^{(L)} \mathrm{e}^{-\lambda_j x} \right) Z_j(0) \mathrm{d}x \\ &= \frac{\omega^2}{g} \sum_{L=1}^{4} \dot{A}_L \sum_{j=1}^{\infty} \frac{\left[A_{5,j}^{(L)} \left(\mathrm{e}^{\lambda_j x_{\mathrm{L},3}} - \mathrm{e}^{\lambda_j x_{\mathrm{R},2}} \right) - B_{5,j}^{(L)} \left(\mathrm{e}^{-\lambda_j x_{\mathrm{L},3}} - \mathrm{e}^{-\lambda_j x_{\mathrm{R},2}} \right) \right] Z_j(0)}{\lambda_j} \\ &= \sum_{L=1}^{4} \dot{A}_L \left(\mathrm{i}\omega a_{4,L} - c_{4,L} \right) \end{aligned}, \tag{23}$$

in which

$$a_{4,L} = \frac{\omega}{g} \mathrm{Im} \left(\sum_{j=1}^{\infty} \frac{\left[A_{5,j}^{(L)} \left(\mathrm{e}^{\lambda_j x_{\mathrm{L},3}} - \mathrm{e}^{\lambda_j x_{\mathrm{R},2}} \right) - B_{5,j}^{(L)} \left(\mathrm{e}^{-\lambda_j x_{\mathrm{L},3}} - \mathrm{e}^{-\lambda_j x_{\mathrm{R},2}} \right) \right] Z_j(0)}{\lambda_j} \right), \tag{24}$$

$$c_{4,L} = -\frac{\omega^2}{g} \mathrm{Re} \left(\sum_{j=1}^{\infty} \frac{\left[A_{5,j}^{(L)} \left(\mathrm{e}^{\lambda_j x_{\mathrm{L},3}} - \mathrm{e}^{\lambda_j x_{\mathrm{R},2}} \right) - B_{5,j}^{(L)} \left(\mathrm{e}^{-\lambda_j x_{\mathrm{L},3}} - \mathrm{e}^{-\lambda_j x_{\mathrm{R},2}} \right) \right] Z_j(0)}{\lambda_j} \right). \tag{25}$$

Therefore, $F_{\mathrm{R}}^{(i)} = \sum_{L=1}^{4} \dot{A}_L \left(\mathrm{i}\omega a_{i,L} - c_{i,L} \right)$ is valid for i=1, 2, 3, 4.

2.4.2 Indirect method for solving hydrodynamic coefficients

wave diffraction

In fact, apart from using the direct method as mentioned in Section 2.4.1, the generalized excitation forces may also be expressed in terms of the radiated wave's far-field coefficients using the Haskind Relation (HR). The excitation force (or the excitation volume flow) acting on a body (or an OWC) that experiences a plane wave propagating from a certain direction is related to the body's (or the OWC's) ability to radiate a wave into just that direction (Falnes, 2002). The generalized wave excitation force after using the HR can be derived as:

$$F_{\mathrm{e}}^{(L)} = \frac{-2\mathrm{i}\rho g A k h A_{1,1}^{(L)} (-1)^{\delta_{4,L}}}{Z_1(0)}, \tag{26}$$

Detail derivation of Eq.(26) is given in Appendix A.

wave radiation

Similar to the expression of the generalized excitation forces using the Haskind Relation, reciprocity relations exist for the radiation damping matrix (Falnes, 2002). By using the reciprocity relations, some of the wave radiation damping and added mass can be written in terms of the radiated wave's Far-Field Coefficients (FFC) as follows:

$$c_{i,L} = \omega\rho kh\left(A_{7,1}^{(i)*}A_{7,1}^{(L)} + A_{1,1}^{(i)*}A_{1,1}^{(L)}\right) \qquad \left(i=1,2,3;L=1,2,3\right),\left(i=L=4\right), \tag{27}$$

$$\mu_{i,L} = \mathrm{i}\rho kh\left(A_{7,1}^{(i)*}A_{7,1}^{(L)} + A_{1,1}^{(i)*}A_{1,1}^{(L)}\right) \qquad \left(i=1,2,3;L=4\right),\left(i=4;L=1,2,3\right), \tag{28}$$

where the superscript * denotes complex-conjugate.

2.5. Power absorption of the hybrid WEC

After solving the wave diffraction/radiation problem and obtaining the hydrodynamic coefficients, the response of the hybrid WEC in frequency domain can be calculated using the following dynamic motion equation:

$$\begin{bmatrix} -\mathrm{i}\omega\left(\mathbf{M}+\mathbf{M}_{\mathrm{a}}+\mathbf{M}_{\mathrm{PTO}}\right)+\left(\mathbf{C}_{\mathrm{d}}+\mathbf{C}_{\mathrm{PTO}}\right)+\mathrm{i}\mathbf{K}_{\mathrm{s}}/\omega & \mathbf{A}_{\mathrm{J}}^{\mathrm{T}} \\ \mathbf{A}_{\mathrm{J}} & \mathbf{0} \end{bmatrix}\begin{Bmatrix} \dot{\boldsymbol{X}} \\ \boldsymbol{F}_{\mathrm{J}} \end{Bmatrix} = \begin{Bmatrix} \boldsymbol{F}_{\mathrm{e}} \\ \mathbf{0} \end{Bmatrix}, \tag{29}$$

where $\mathbf{M}$ is the mass matrix; $\mathbf{M}_{\mathrm{a}}$ and $\mathbf{C}_{\mathrm{d}}$ are the added mass matrix and radiation damping matrix, respectively; $\mathbf{M}_{\mathrm{PTO}}$ and $\mathbf{C}_{\mathrm{PTO}}$ are the mass matrix and damping matrix, respectively, induced by the PTO system; $\mathbf{K}_{\mathrm{s}}$ is the hydrostatic restoring matrix; $\mathbf{A}_{\mathrm{J}}$ is the constraint matrix due to the hinge restriction to the float; the superscript T denotes transpose; $\dot{\boldsymbol{X}} = \begin{bmatrix} \dot{A}_1 & \dot{A}_2 & \dot{A}_3 & \dot{A}_4 \end{bmatrix}^{\mathrm{T}}$ represents the velocity response vector of the hybrid WEC to be determined; $\boldsymbol{F}_{\mathrm{J}}$ denotes the hinge force vector; $\boldsymbol{F}_{\mathrm{e}}$ is the generalized wave excitation force vector.

$$\mathbf{A}_{\mathrm{J}} = \begin{bmatrix} 1 & 0 & d & 0 \\ 0 & 1 & -D & 0 \end{bmatrix},\ \mathbf{M} = \begin{bmatrix} m & & & \\ & m & & \\ & & I & \\ & & & 0 \end{bmatrix},\ \mathbf{K}_{\mathrm{s}} = \rho g \begin{bmatrix} 0 & & & \\ & a_1 & & \\ & & \frac{a_1^3}{12} - \frac{a_1 d_1^2}{2} & \\ & & & 0 \end{bmatrix},$$

$$\mathbf{C}_{\mathrm{PTO}} = \begin{bmatrix} 0 & & & \\ & 0 & & \\ & & c_1 & \\ & & & c_2 \end{bmatrix},\ \mathbf{M}_{\mathrm{PTO}} = \begin{bmatrix} 0 & & & \\ & 0 & & \\ & & 0 & \\ & & & \frac{V_0}{c_a^2\rho_0} \end{bmatrix}, \tag{30}$$

in which m is the mass of the float; I is the rotary inertia of the float relative to the centre of mass; c_1 and c_2 represent the linear damping of the hydraulic cylinder and the OWC turbine PTO system, respectively; V_0 is the air chamber volume; c_a is the sound velocity in air; ρ_0 is the static

air density. In subsequent computations, ρ/ρ_0=800, c_a =340m/s and the air chamber volume is $V_0=2a^2$ unless otherwise specified.

Wave power is absorbed by the damping in both the float PTO system and the OWC PTO system. After solving Eq.(29), $\dot{\boldsymbol{X}}$ is obtained and the average power that the hybrid WEC captures from regular waves can be written as

$$P=\frac{1}{2}\left(c_1\left|\dot{A}_3\right|^2+c_2\left|\dot{A}_4\right|^2\right). \tag{31}$$

The power absorption efficiency is calculated as:

$$\eta=\frac{P}{0.5\rho g A^2 c_g}, \tag{32}$$

where $c_g=\frac{\omega}{2k}\left[1+\frac{2kh}{\sinh\left(2kh\right)}\right]$.

2.6. Optimization of power absorption

The power absorption capability of a WEC is a particular subject of interest. As described above, although surge, heave and pitch modes of the float are all included in the float motion, only the pitch motion, together with the oscillation of water column, are used to drive PTO systems. Thanks to the mechanical relation between the surge, heave and pitch modes of the float induced by the hinge constraints, Eq. (29) can be reduced to the solution of a 2-order algebraic matrix equation with the employment of matrix blocking method as follows.

Matrix $\left[-\mathrm{i}\omega\left(\mathbf{M}+\mathbf{M}_{\mathrm{a}}+\mathbf{M}_{\mathrm{PTO}}\right)+\left(\mathbf{C}_{\mathrm{d}}+\mathbf{C}_{\mathrm{PTO}}\right)+\mathrm{i}\mathbf{K}_{\mathrm{s}}/\omega\right]$ can be partitioned into four blocks $\mathbf{S}_{11}$, $\mathbf{S}_{12}$, $\mathbf{S}_{21}$, and $\mathbf{S}_{22}$ whose sizes are all 2×2. The hinge force vector $\boldsymbol{F}_{\mathrm{J}}$ can be expressed in terms of wave excitation forces loading on the float in surge and heave modes, and the velocity response of both the float in pitch mode and the air pressure inside the chamber as

$$\boldsymbol{F}_{\mathrm{J}}=\begin{Bmatrix}F_{\mathrm{e}}^{(1)}\\F_{\mathrm{e}}^{(2)}\end{Bmatrix}-\begin{bmatrix}\mathbf{S}_{11} & \mathbf{S}_{12}\end{bmatrix}\begin{bmatrix}\mathbf{A}_{\mathrm{T}}\\\mathbf{I}\end{bmatrix}\begin{Bmatrix}\dot{A}_3\\\dot{A}_4\end{Bmatrix}=\begin{Bmatrix}F_{\mathrm{e}}^{(1)}\\F_{\mathrm{e}}^{(2)}\end{Bmatrix}-\left(\mathbf{S}_{11}\mathbf{A}_{\mathrm{T}}+\mathbf{S}_{12}\right)\begin{Bmatrix}\dot{A}_3\\\dot{A}_4\end{Bmatrix}, \tag{33}$$

where $\mathbf{A}_{\mathrm{T}}=\begin{bmatrix}-d & 0\\D & 0\end{bmatrix}$.

In addition, $\boldsymbol{F}_{\mathrm{J}}$, $\dot{A}_3$, $\dot{A}_4$, $F_{\mathrm{e}}^{(3)}$ and $F_{\mathrm{e}}^{(4)}$ should also satisfy the following relation:

$$\begin{bmatrix}\mathbf{S}_{21} & \mathbf{S}_{22}\end{bmatrix}\begin{bmatrix}\mathbf{A}_{\mathrm{T}}\\\mathbf{I}\end{bmatrix}\begin{Bmatrix}\dot{A}_3\\\dot{A}_4\end{Bmatrix}-\mathbf{A}_{\mathrm{T}}^{\mathrm{T}}\boldsymbol{F}_{\mathrm{J}}=\left(\mathbf{S}_{21}\mathbf{A}_{\mathrm{T}}+\mathbf{S}_{22}\right)\begin{Bmatrix}\dot{A}_3\\\dot{A}_4\end{Bmatrix}-\mathbf{A}_{\mathrm{T}}^{\mathrm{T}}\boldsymbol{F}_{\mathrm{J}}=\begin{Bmatrix}F_{\mathrm{e}}^{(3)}\\F_{\mathrm{e}}^{(4)}\end{Bmatrix}. \tag{34}$$

Submitting Eqs. (33-34) into Eq. (29) and making some rearrangements gives

$$\left(\mathbf{A}_{\mathrm{T}}^{\mathrm{T}}\mathbf{S}_{11}\mathbf{A}_{\mathrm{T}}+\mathbf{A}_{\mathrm{T}}^{\mathrm{T}}\mathbf{S}_{12}+\mathbf{S}_{21}\mathbf{A}_{\mathrm{T}}+\mathbf{S}_{22}\right)\begin{Bmatrix}\dot{A}_3\\ \dot{A}_4\end{Bmatrix}=\begin{Bmatrix}F_{\mathrm{e}}^{(3)}\\ F_{\mathrm{e}}^{(4)}\end{Bmatrix}+\mathbf{A}_{\mathrm{T}}^{\mathrm{T}}\begin{Bmatrix}F_{\mathrm{e}}^{(1)}\\ F_{\mathrm{e}}^{(2)}\end{Bmatrix}, \tag{35}$$

in which the PTO damping coefficients (c_1 and c_2) can be easily separated, and Eq. (35) can be rewritten into a 2-order linear matrix equation:

$$\begin{bmatrix}A_0+c_1 & B_0\\ C_0 & D_0+c_2\end{bmatrix}\begin{Bmatrix}\dot{A}_3\\ \dot{A}_4\end{Bmatrix}=\begin{Bmatrix}E_0\\ F_0\end{Bmatrix}, \tag{36}$$

where the subscript "0" of A_0~F_0 means that these parameters are independent of c_1 and c_2.

After expressing $\dot{A}_3$ and $\dot{A}_4$ in terms of A_0~F_0, c_1 and c_2, and submitting them into Eq. (31), we have the new expression of P as a two variable explicit function

$$P(c_1,c_2)=\frac{1}{2}\frac{c_1\left(u_1c_2^2+u_2c_2+u_3\right)+c_2\left(u_4c_1^2+u_5c_1+u_6\right)}{c_1^2c_2^2+u_7c_1^2c_2+u_8c_1c_2^2+u_9c_1^2+u_{10}c_2^2+u_{11}c_1c_2+u_{12}c_1+u_{13}c_2+u_{14}}, \tag{37}$$

where u_1~u_{14} are expressed in terms of A_0~F_0: $u_1=|E_0|^2$, $u_2=2\mathrm{Re}\left[E_0^*\left(D_0E_0-B_0F_0\right)\right]$,

$u_3=|D_0E_0-B_0F_0|^2$, $u_4=|F_0|^2$, $u_5=2\mathrm{Re}\left[F_0^*\left(A_0F_0-C_0E_0\right)\right]$, $u_6=|A_0F_0-C_0E_0|^2$, $u_7=2\mathrm{Re}(D_0)$,

$u_8=2\mathrm{Re}(A_0)$, $u_9=|D_0|^2$, $u_{10}=|A_0|^2$, $u_{11}=2\mathrm{Re}\left(A_0D_0-B_0C_0+A_0D_0^*\right)$,

$u_{12}=2\mathrm{Re}\left[D_0^*\left(A_0D_0-B_0C_0\right)\right]$, $u_{13}=2\mathrm{Re}\left[A_0^*\left(A_0D_0-B_0C_0\right)\right]$, $u_{14}=|A_0D_0-B_0C_0|^2$.

The frequency dependent maximum of absorbed power, denoted as P_0 (ω), can be achieved when $\partial P/\partial c_1=0$ and $\partial P/\partial c_2=0$. While for some rare cases, the maximum value of P may occur at either c_1 or c_2 being 0 or $+\infty$.

For c_2=0, $P=\frac{1}{2}\frac{u_3c_1}{u_9c_1^2+u_{12}c_1+u_{14}}$ and the maximum absorbed power, denoted as P_1, occurs if

$c_1=\sqrt{u_{14}/u_9}$, for which we have $P_1=\frac{1}{2}\frac{u_3\sqrt{u_{14}/u_9}}{2u_{14}+u_{12}\sqrt{u_{14}/u_9}}$;

For c_1=0, $P=\frac{1}{2}\frac{u_6c_2}{u_{10}c_2^2+u_{13}c_2+u_{14}}$ and the maximum absorbed power, denoted as P_2, occurs if

$c_2=\sqrt{u_{14}/u_{10}}$, for which we have $P_2=\frac{1}{2}\frac{u_6\sqrt{u_{14}/u_{10}}}{2u_{14}+u_{13}\sqrt{u_{14}/u_{10}}}$;

For c_2=+∞, $P=\frac{1}{2}\frac{u_1 c_1}{c_1^2+u_8 c_1+u_{10}}$ and the maximum absorbed power, denoted as P_3, occurs if $c_1=\sqrt{u_{10}}$, for which we have $P_3=\frac{1}{2}\frac{u_1\sqrt{u_{10}}}{2u_{10}+u_8\sqrt{u_{10}}}$;

For c_1=+∞, $P=\frac{1}{2}\frac{u_4 c_2}{c_2^2+u_7 c_2+u_9}$ and the maximum absorbed power, denoted as P_4, occurs if $c_2=\sqrt{u_9}$, for which we have $P_4=\frac{1}{2}\frac{u_4\sqrt{u_9}}{2u_9+u_7\sqrt{u_9}}$.

In summary, the maximum absorbed power by the hybrid WEC, denoted as $P_{\max}$ is

$$P_{\max}=\max\left(P_0,P_1,P_2,P_3,P_4\right). \tag{38}$$

The maximum power absorption efficiency for $P_{\max}$ can be calculated in a similar way as given in Eq. (32), which is notated by $\eta_{\max}$. The corresponding optimized PTO damping for the float and the OWC are notated by $c_{\mathrm{opt},1}$ and $c_{\mathrm{opt},2}$, respectively.

2.7. Wave reflection and transmission coefficients

The spatial velocity potential in the distance far away from the hybrid WEC can be written as:

$$\Phi\left(-x_\infty,0\right)=-\frac{\mathrm{i}g}{\omega}\frac{Z_1(z)}{Z_1(0)}\left[A\mathrm{e}^{-\mathrm{i}kx_\infty}+\frac{\mathrm{i}\omega}{g}Z_1(0)\left(A_{1,1}^{\mathrm{D}}+\sum_{L=1}^{4}\dot{A}^{(L)}A_{1,1}^{\mathrm{R},L}\right)\mathrm{e}^{\mathrm{i}kx_\infty}\right], \tag{39}$$

$$\Phi\left(x_\infty,0\right)=-\frac{\mathrm{i}g}{\omega}\frac{Z_1(z)}{Z_1(0)}\left[A\mathrm{e}^{\mathrm{i}kx_\infty}+\frac{\mathrm{i}\omega}{g}Z_1(0)\left(A_{7,1}^{\mathrm{D}}+\sum_{L=1}^{4}\dot{A}^{(L)}A_{7,1}^{\mathrm{R},L}\right)\mathrm{e}^{\mathrm{i}kx_\infty}\right]. \tag{40}$$

Therefore, the wave reflection coefficient and the wave transmission coefficient of the WEC, denoted as R and T, respectively, can be calculated as:

$$R=\left|\frac{\omega}{gA}Z_0(0)\left(A_{1,1}^{\mathrm{D}}+\sum_{L=1}^{4}\dot{A}^{(L)}A_{1,1}^{\mathrm{R},L}\right)\right|, \tag{41}$$

$$T=\left|1+\frac{\mathrm{i}\omega}{gA}Z_0(0)\left(A_{7,1}^{\mathrm{D}}+\sum_{L=1}^{4}\dot{A}^{(L)}A_{7,1}^{\mathrm{R},L}\right)\right|. \tag{42}$$

3. Model validation

To validate the solutions of wave diffraction and radiation problems in the analytical model as described in Section 2, wave excitation forces/volume flux, added mass and radiation damping are all evaluated by using both direct method and indirect method. By checking these results of

the certain hydrodynamic parameters using different methods, the solutions of wave diffraction and radiation problems can be validated if good agreements are satisfied. What is more, hydrodynamic performance of an OWC consisting of two vertical thin barriers with unequal length is also evaluated and is compared with published results (Falnes and McIver, 1985). The theoretical maximum power absorption of the hybrid WEC, wave reflection and transmission coefficients can be validated by comparing with the results from trial-and-error method and by checking the energy conservation identity, respectively.

The excitation forces/volume flux and hydrodynamic coefficients together with both float PTO damping and OWC PTO damping are normalized as follows:

$$\bar{F}_{\mathrm{e}}^{(j)}=\begin{cases}\dfrac{\left|F_{\mathrm{e}}^{(j)}\right|}{\rho g A h},\ j=1,2\\ \dfrac{\left|F_{\mathrm{e}}^{(j)}\right|}{\rho g A h^{2}},\ j=3\\ \dfrac{\left|F_{\mathrm{e}}^{(j)}\right|}{A\sqrt{gh}},\ j=4\end{cases},\qquad \bar{c}_{i,j}=\begin{cases}\dfrac{c_{i,j}}{\rho h\sqrt{gh}},\ i=1,2;\ j=1,2\\ \dfrac{c_{i,j}}{\rho h^{2}\sqrt{gh}},\ (i=1,2;\ j=3),(i=3;\ j=1,2)\\ \dfrac{c_{i,j}}{h},\ (i=1,2;\ j=4),(i=4;\ j=1,2)\\ \dfrac{c_{i,j}}{\rho h^{3}\sqrt{gh}},\ i=j=3\\ \dfrac{c_{i,j}}{h^{2}},\ (i=3;\ j=4),(i=4;\ j=3)\\ \dfrac{\rho g c_{i,j}}{\sqrt{gh}},\ i=j=4\end{cases},$$

$$\bar{\mu}_{i,j}=\begin{cases}\dfrac{\omega\mu_{i,j}}{\rho h\sqrt{gh}},\ i=1,2;\ j=1,2\\ \dfrac{\omega\mu_{i,j}}{\rho h^{2}\sqrt{gh}},\ (i=1,2;\ j=3),(i=3;\ j=1,2)\\ \dfrac{\omega\mu_{i,j}}{h},\ (i=1,2;\ j=4),(i=4;\ j=1,2)\\ \dfrac{\omega\mu_{i,j}}{\rho h^{3}\sqrt{gh}},\ i=j=3\\ \dfrac{\omega\mu_{i,j}}{h^{2}},\ (i=3;\ j=4),(i=4;\ j=3)\\ \dfrac{\omega\rho g\mu_{i,j}}{\sqrt{gh}},\ i=j=4\end{cases},$$

$$\bar{\dot{x}}=\frac{\dot{x}\sqrt{gh}}{Ag},\quad \bar{p}=\frac{p}{\rho g A},\quad \bar{c}_{\mathrm{opt}}^{(1)}=\frac{c_{\mathrm{opt},1}}{\rho h^{3}\sqrt{gh}},\quad \bar{c}_{\mathrm{opt}}^{(2)}=\frac{\rho g c_{\mathrm{opt},2}}{\sqrt{gh}}.$$

Figure 3 gives the results of wave excitation forces/volume flux for the hybrid WEC with a_1/h=0.1, a_2/h= a_3/h=0.005, d_1/h=0.025, d_2/h=0.1, d_3/h=0.15, D/h=0.15, a/h=0.1. The corresponding wave damping and added mass are illustrated in Figs. 4 and 5, respectively.

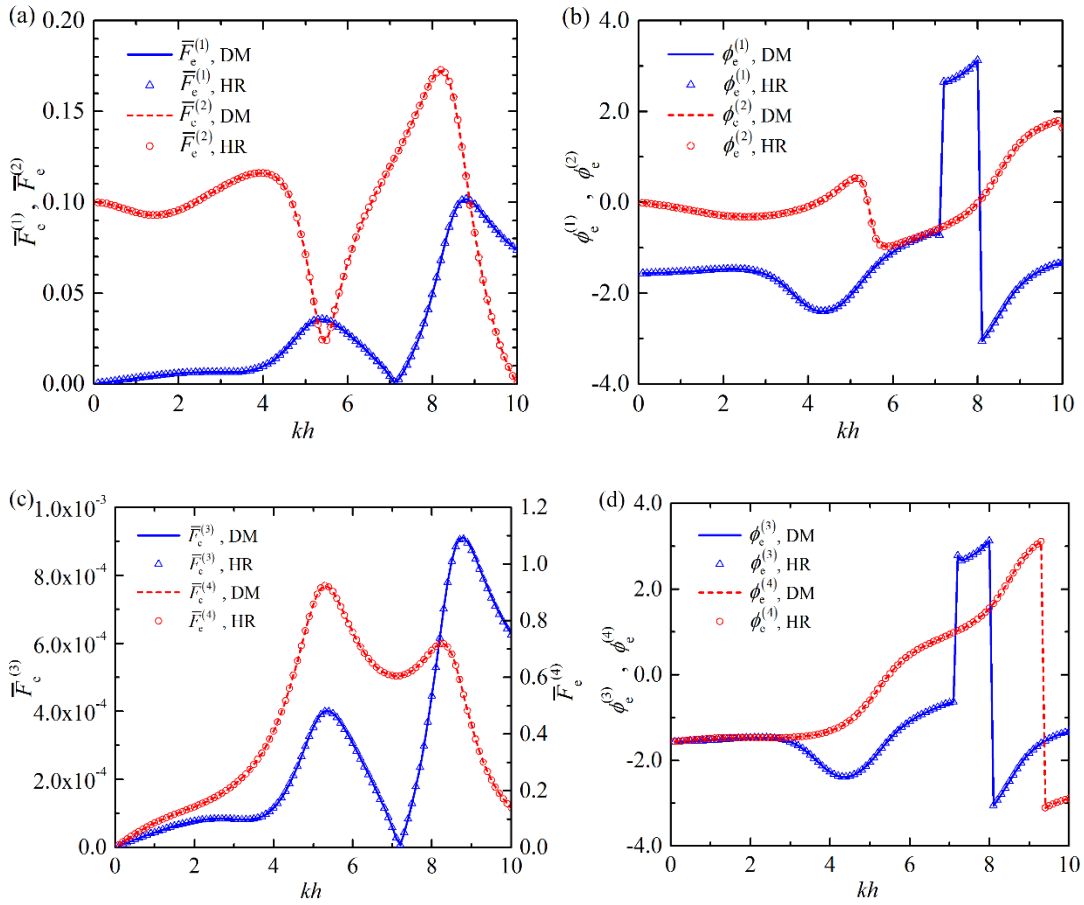

Fig. 3 Wave excitation forces/volume flux for a_1/h=0.1, a_2/h= a_3/h=0.005, d_1/h=0.025, d_2/h=0.1, d_3/h=0.15, D/h=0.15, a/h=0.1: (a) Dimensionless magnitudes of surge and heave wave excitation forces acting on the float; (b) Phases of surge and heave wave excitation forces acting on the float; (c) Dimensionless magnitudes of pitch wave excitation force acting on the float and wave excitation volume flux of the OWC; (d) Phases of pitch wave excitation force acting on the float and wave excitation volume flux of the OWC.

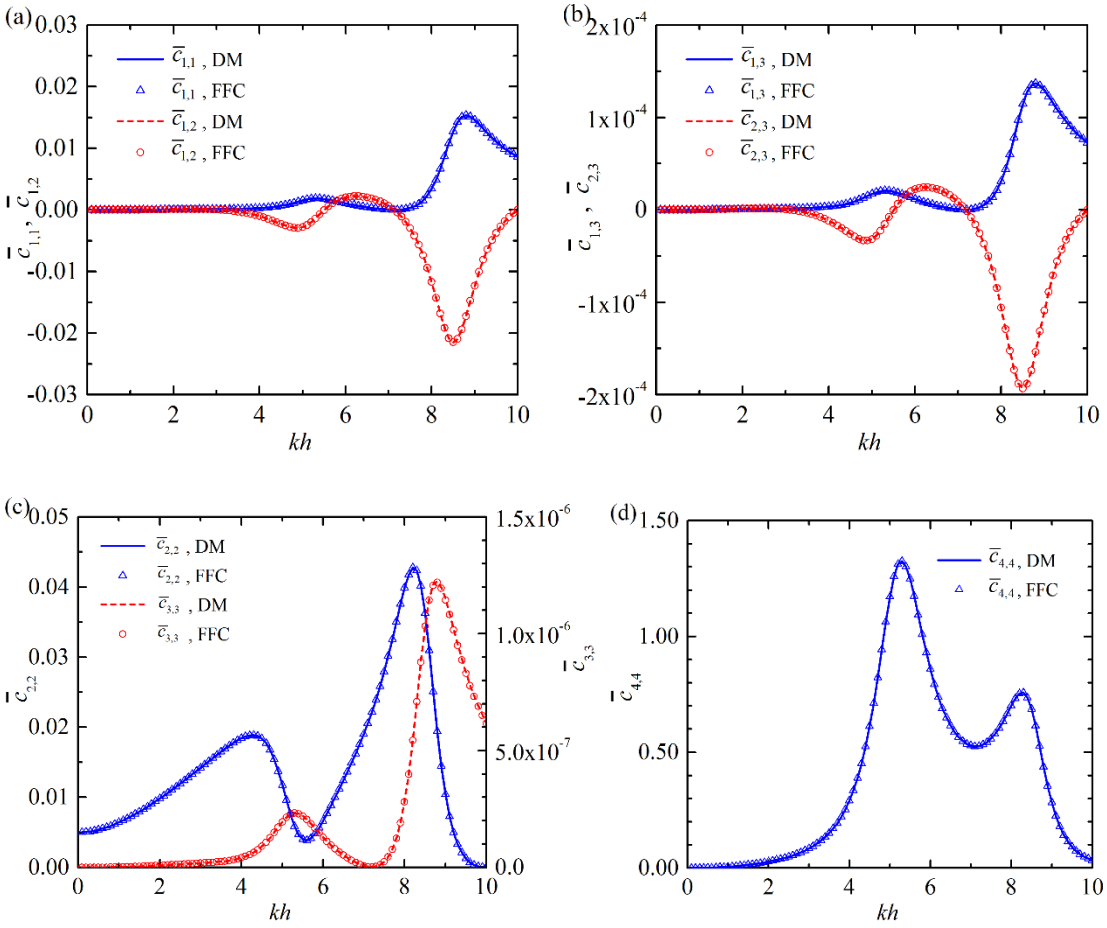

Fig. 4 Wave radiation damping for a_1/h=0.1, a_2/h= a_3/h=0.005, d_1/h=0.025, d_2/h=0.1, d_3/h=0.15, D/h=0.15, a/h=0.1: (a) Wave radiation damping of the float in surge mode due to the oscillation of the float in surge and heave modes; (b) Wave radiation damping of the float in surge and heave modes due to the oscillation of the float in pitch mode; (c) Wave radiation damping of the float in heave and pitch modes due to the oscillation of the float in heave and pitch modes, respectively; (d) Wave radiation damping of the OWC due to the air pressure oscillation inside the OWC chamber.

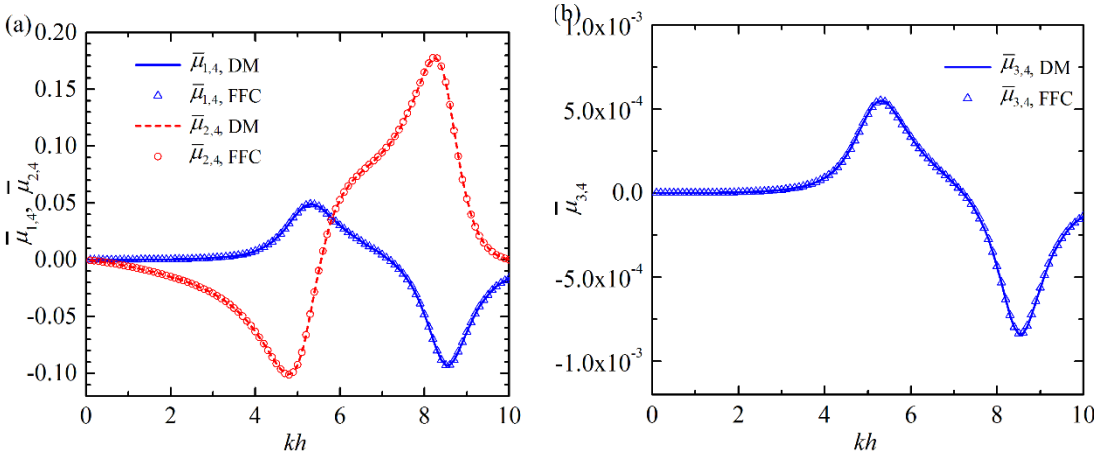

Fig. 5 Added mass for a_1/h=0.1, a_2/h= a_3/h=0.005, d_1/h=0.025, d_2/h=0.1, d_3/h=0.15, D/h=0.15, a/h=0.1: (a) Added mass of the float in surge and heave modes due to the air pressure oscillation inside the OWC chamber; (b) Added mass of the float in pitch mode due to the air pressure oscillation inside the OWC chamber.

As shown in Figs. 3~5, results of the wave excitation forces/volume flux, wave damping and added mass of the hybrid WEC by using direct and indirect methods agree perfectly with each other.

Previously, Falnes and McIver (1985) used to study the power absorption by an OWC, which is composed of two vertical thin barriers with unequal length. Here, after setting the float width, float submergence depth and thickness of both fore wall and aft wall of OWC chamber to rather small values, the hybrid WEC looks rather similar with the device studied by Falnes and McIver (1985). The obtained results of wave excitation volume flux and the corresponding hydrodynamic coefficients for $a_1/h=a_2/h=a_3/h$=0.001, d_1/h=0.001, d_2/h=0.15, d_3/h=0.25, D/h=0.001, a/h=0.1 are compared with those from Falnes and McIver (1985) in Figs. 6 and 7.

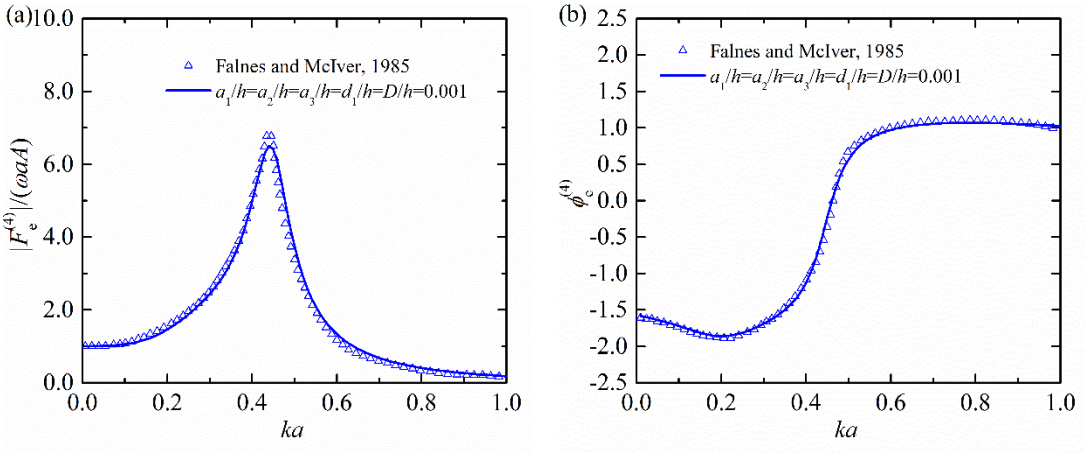

Fig. 6 Dimensionaless excitation volume flux versus *ka* for the chosen geometrical parameters: d_2/h=0.15, d_3/h=0.25, a/h=0.1. (a) Amplitude; (b) Phase. (Normalizing principle adopted by Falnes and McIver (1985) is applied to the present figure)

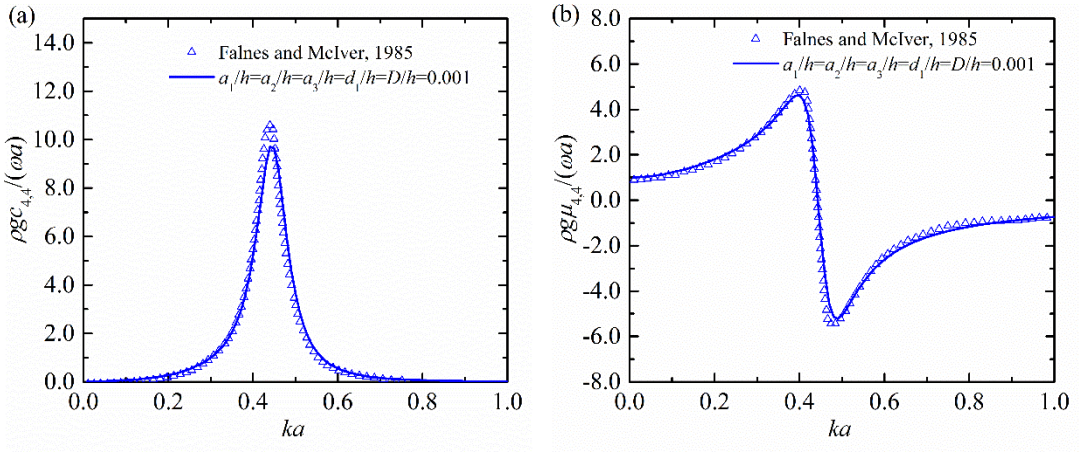

Fig. 7 Dimensionaless radiation damping and added mass versus *ka* for the chosen geometrical parameters: d_2/h=0.15, d_3/h=0.25, a/h=0.1. (a) Radiation damping coefficient; (b) Added mass coefficient. (Normalizing principle adopted by Falnes and McIver (1985) is applied to the present figure)

The good agreement between the obtained results and those from Falnes and McIver (1985) is also obtained as plotted in Figs. 6 and 7. It can be learnt from Figs. 3~7 that the present analytical model performs quite well in solving wave diffraction and radiation problems of the hybrid WEC.

Figure 8a illustrates the comparison between the analytical results of the maximum power absorption efficiency and the numerical ones using trial-and-error method for a_1/h=0.1, a_2/h= a_3/h=0.005, d_1/h=0.025, d_2/h=0.1, d_3/h=0.15, D/h=0.15, a/h=0.1, d/h=0.05. The trial-and-error method is adopted for searching the maximum efficiency in the frame of $\overline{c}^{(1)} \in [0, 0.025]$ and $\overline{c}^{(2)} \in [0, 8.0]$. The corresponding optimized float PTO damping and OWC PTO damping are also given in Fig.8b. Analytical and numerical results of $\eta_{\max}$, $\overline{c}_{\text{opt}}^{(1)}$ and $\overline{c}_{\text{opt}}^{(2)}$ are found to be in very good agreement for different wave conditions.

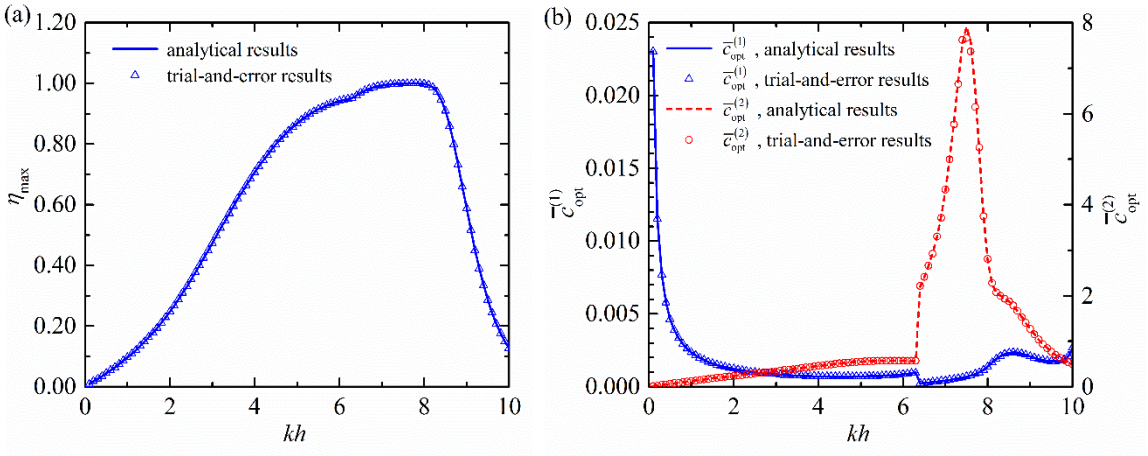

Fig.8 Variation of $\eta_{\max}$, $\bar{c}_{\text{opt}}^{(1)}$ and $\bar{c}_{\text{opt}}^{(2)}$ with kh for a_1/h=0.1, a_2/h= a_3/h=0.005, d_1/h=0.025, d_2/h=0.1, d_3/h=0.15, D/h=0.15, a/h=0.1, d/h=0.05: (a) $\eta_{\max}$; (b) $\bar{c}_{\text{opt}}^{(1)}$ and $\bar{c}_{\text{opt}}^{(2)}$.

Figure 9 shows the results of η, R, T and $\eta+R^2+T^2$ varying with kh for a_1/h=0.1, a_2/h= a_3/h=0.005, d_1/h=0.025, d_2/h=0.1, d_3/h=0.15, D/h=0.15, a/h=0.1, d/h=0.05, $\bar{c}^{(1)}$=0.001 and $\bar{c}^{(2)}$ =0.5. The energy conservation relationship $\eta+R^2+T^2$=1 is satisfied perfectly, which indirectly validates the present analytical model as well.

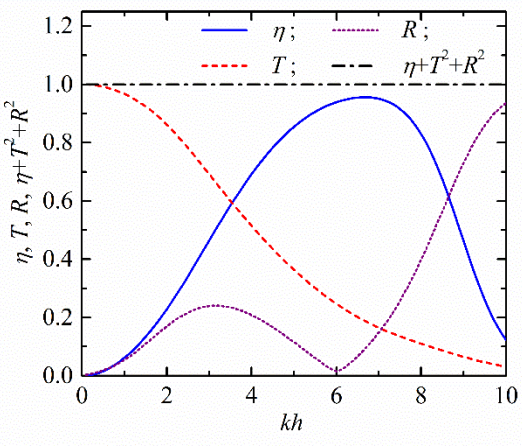

Fig.9 Variation of η, R, T and $\eta+R^2+T^2$ with kh for a_1/h=0.1, a_2/h= a_3/h=0.005, d_1/h=0.025, d_2/h=0.1, d_3/h=0.15, D/h=0.15, a/h=0.1, d/h=0.05, $\bar{c}^{(1)}$=0.001 and $\bar{c}^{(2)}$ =0.5.

Although the hybrid WEC can be used as a kind of floating breakwaters by reducing amplitude of the wave transmitted far behind the device, in the following sections, the study is mainly focused on the performance in wave power exploitation.

4. Model Application

4.1. Comparison between the hybrid WEC and the isolated float and OWC

To study the influence of the hydrodynamic interaction between the float and the OWC on power absorption of the hybrid WEC, the wave power absorbed by the isolated float and OWC working in open sea, as show in Fig. 10, are also evaluated, respectively, as a comparison with that of the hybrid WEC.

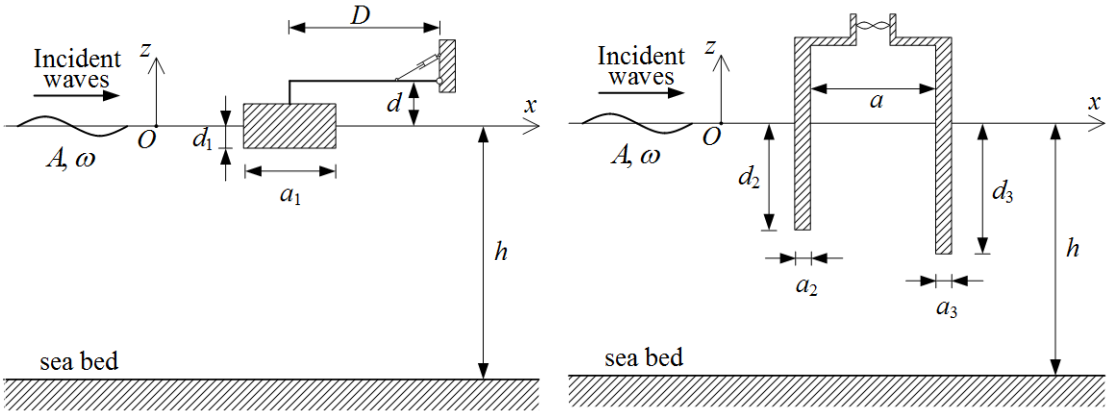

Fig. 10 Sketches of the isolated OWC and the isolated hinged float: (a) isolated float; (b) isolated OWC

The wave excitation forces and hydrodynamic coefficients of an isolated float (as shown in Fig.10a) can be evaluated using the analytical model proposed by Zheng et al. (2014). Analytical solution of wave diffraction and radiation by the isolated OWC (as shown in Fig.10b) can be derived base on the study carried out by Zheng and Zhang (2016). As both the oscillating motion of the isolated float and that of the isolated OWC can be treated as an oscillating system with only one degree of freedom, the maximized absorbed power and the corresponding optimal PTO damping for each situation can be calculated quite easily by solving a partial differential equation of single degree of freedom (Falnes, 2002).

Figure 11 illustrates the frequency response comparison of the maximum power capture efficiency of the hybrid WEC and those of the hinged float and the OWC when they are independently deployed for a_1/h=0.1, a_2/h= a_3/h=0.005, d_1/h=0.025, d_2/h=0.1, d_3/h=0.15, D/h=0.15, a/h=0.1, d/h=0.05. For kh<10, the maximum power capture efficiency of the hinged float, $\eta_{\max}^{(1)}$, is no more than 0.3. While as kh increases from 0 to 10, the maximum efficiency of the isolated OWC, $\eta_{\max}^{(2)}$, first increases and then decreases after reaching the peak value of 0.87 at kh=6.0 with a narrow bandwidth. $\eta_{\max}^{(2)}$>0.8 only occurs at 5.7<kh<6.4. After combining these segments together, i.e., the hybrid WEC, the power extraction capacity is significantly improved. For 7.1<kh<8.0, almost all the incident power can be captured when the PTO damping coefficients are optimized. What is better, the frequency bandwidth for $\eta_{\max}$>0.8 is 4.6<kh<8.7, much wider than that of the isolated OWC. It is very interesting to find that if the hinged float in the absence of the OWC and the OWC in the absence of the hinged float are considered, respectively, the efficiency of both of them ($\eta_{\max}^{(1)}+\eta_{\max}^{(2)}$) is smaller than the efficiency of the hybrid WEC ($\eta_{\max}$) for 1.4<kh<5.1 and 6.7<kh<9.0, as shown in Fig.11. And the frequency bandwidth of $\eta_{\max}$ of the hybrid WEC is larger than those of both the isolated hinged float and isolated OWC ($\eta_{\max}^{(1)}+\eta_{\max}^{(2)}$) for $\eta>50\%$. This means that the hydrodynamic interaction between the float and the OWC plays a positive effect on both the power absorption for some range of

wave conditions and frequency response width of the hybrid WEC. Although the peak value of η_{max} of the hybrid WEC is smaller than that of both the isolated hinged float and isolated OWC, it is believed that the hybrid WEC can be used to a wider range of wave conditions with a rather high power absorption efficiency. In the random waves with more incident power distributed at $1.4<kh<5.1$ and $6.7<kh<9.0$, output power of the hybrid WEC could be larger than the sum of output power of both the isolated hinged float and isolated OWC.

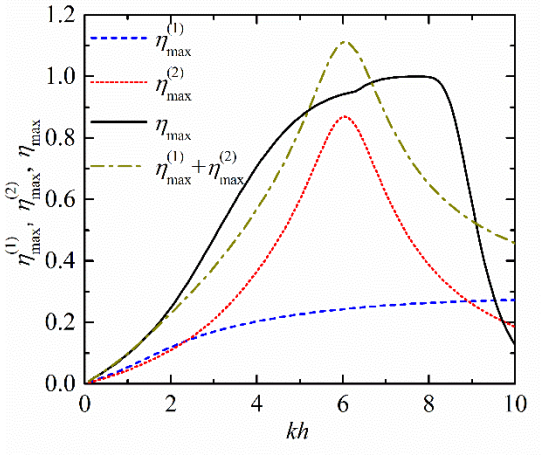

Fig. 11 Variation of η_{max}, $\eta_{max}^{(1)}$ and $\eta_{max}^{(2)}$ with kh for a_1/h=0.1, a_2/h= a_3/h=0.005, d_1/h=0.025, d_2/h=0.1, d_3/h=0.15, D/h=0.15, a/h=0.1, d/h=0.05.

4.2. Impact analysis on power absorption by multiple parameters

4.2.1 Effect of OWC chamber width

Figure 12 shows the frequency response of η_{max} for various OWC chamber widths (a/h). Due to the existence of the hinged float, the η_{max}-kh curve of the hybrid WEC could hold more peaks with some specified structural dimensions (as given in Fig. 12), rather than merely one single peak for an isolated stationary offshore OWC (Elhanafi et al., 2017). For $kh<5.0$, the larger a/h is, the larger η_{max} by the hybrid WEC can be achieved whereas when $6.0<kh<6.5$ a/h shows the opposite effect on η_{max}. It is noted that once a/h is doubled from 0.05 to 0.10, the maximum increase in η_{max} can reach 40%. However, the influence of a/h on η_{max} is not obvious for long wave length and short wave length, such as $kh<2.5$ and $kh>7.5$. As OWC chamber width (a/h) increases from 0.05 to 0.15, the value of kh, where the second peak of η_{max}-kh curve occurs, decreases from 6.7 to 5.3.

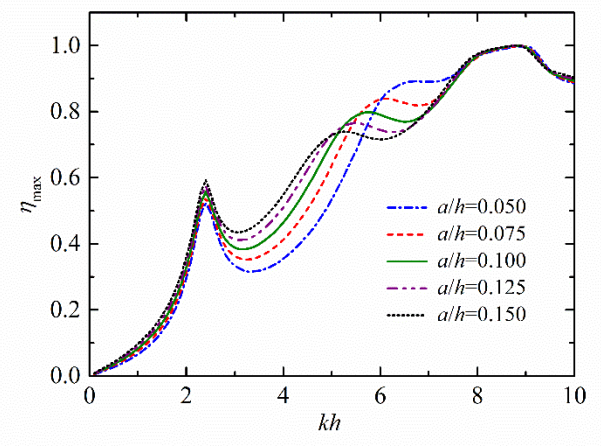

Fig. 12 Variation of η_{max} for various OWC chamber width (a/h) with a_1/h=0.05, a_2/h= a_3/h=0.005, d_1/h=0.05, d_2/h=0.1, d_3/h=0.15, D/h=0.1, d/h=0.1.

4.2.2 Effect of submergence of the OWC side walls

The frequency response of η_{max} for various submergences of the OWC fore wall (d_2/h) is plotted in Fig. 13. It shows that, for kh<4.0, a larger value of d_2/h is welcome for capturing power from waves. This result is consistent with the corresponding numerical one for an offshore stationary OWC, that the energy extraction in long waves can be improved with the increase of the submergence of lips (Elhanafi et al., 2017). Compared to the other device with a larger d_2/h, the hybrid WEC with the smallest d_2/h (=0.05) has the least power capture capacity for all the wave conditions studied (kh<10). However, increasing d_2/h will not play a positive effect on power absorption for all kh. For example, when kh=5.8, the corresponding η_{max} is 0.8 for d_2/h=0.10, which is obviously larger than those for d_2/h=0.05, 0.15, and 0.20.

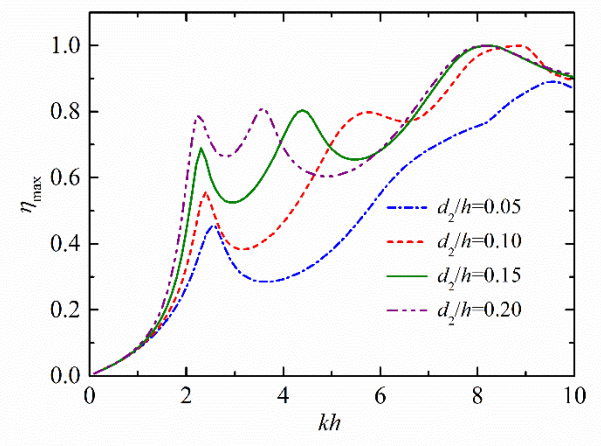

Fig. 13 Variation of η_{max} for various submergence of the OWC side walls (d_2/h) with a_1/h=0.05, a_2/h= a_3/h=0.005, d_1/h=0.05, d_3/h=d_2/h+0.05, a/h=0.1, D/h=0.1, d/h=0.1.

4.2.3 Effect of float width

As another vital parameter affecting power absorption of the hybrid WEC, influence of float width (a_1/h) is illustrated in Fig. 14. It can be learned that the first and second peaks of the η_{max}-kh curve, occurring at $1.0<kh<4.0$ and $4.4<kh<7.2$, respectively, both are quite sensitive to a_1/h. The larger a_1/h is, the larger the first peak value of η_{max} and the corresponding kh are, whereas the larger a_1/h is, the smaller the second peak value of η_{max} and the corresponding kh are. While for $4.4<kh<7.2$, more power can be absorbed by the hybrid WEC with a smaller a_1/h. Thus, within $kh\in[1.0, 7.2]$ in which the water depth is specifically given, for waves with a smaller wave length (or high wave frequency) there is a demand to deploy a hybrid WEC device with a smaller a_1/h to realize more power absorption whereas for waves with a larger wave length there is a demand to deploy a hybrid WEC device generally with a larger a_1/h, which is mainly due to its larger peak value of power absorption efficiency and wider response width.

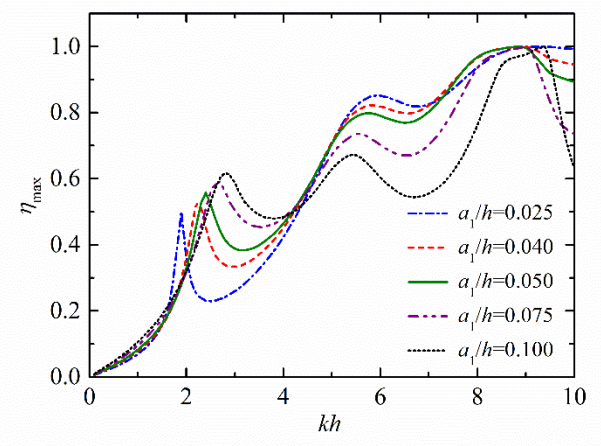

Fig. 14 Variation of η_{max} for various float width (a_1/h) with a_2/h= a_3/h=0.005, d_1/h=0.05, d_2/h=0.1, d_3/h=0.15, a/h=0.1, D/h=0.1, d/h=0.1.

4.3.4 Effect of float draft

Figure 15 shows the variation of η_{max} with kh for various float draft (d_1/h) ranging from 0.025 to 0.1. For d_1/h=0.025, as kh increases from 0 to 10, η_{max} first increases and then tends to be stable after reaching 0.95 at kh=5.4. As a comparison, the η_{max}-kh curves representing the rest cases with a larger d_1/h are quite different from that for d_1/h=0.025. A sharp peak happens at $0<kh<3.0$ for d_1/h=0.050, 0.075, and 0.100, respectively. The hybrid WEC with a larger d_1/h means a smaller first resonant frequency of the float, therefore the sharp peak moves toward the left side of the kh axis. It can be seen that for waves with long wave length, there is a need of a larger d_1/h to match waves so as to acquire a larger η_{max}, but this is at the expense of narrowing the frequency response width. Therefore, for waves with long wave length and a certain frequency width, even though the natural frequency of the device matches the waves to obtain the peak value of η_{max}, the total power absorbed by the WEC is still quite limited due to a narrower frequency response bandwidth. It can be seen clearly that, for waves with short wave length (or

high wave frequency) and a certain frequency width, wave energy is converted efficiently, and the smaller the float draft (d_1/h) is, generally the larger the total power absorbed is.

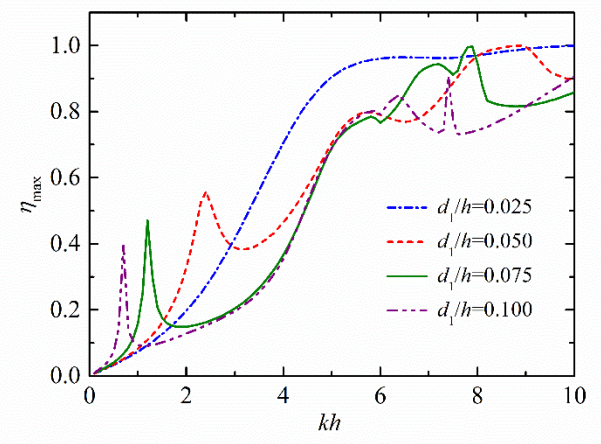

Fig. 15 Variation of η_{max} for various float draft (d_1/h) with a_1/h=0.05, a_2/h= a_3/h=0.005, d_2/h=0.1, d_3/h=0.15, a/h=0.1, D/h=0.1, d/h=0.1.

4.3.5 Effect of the distance between float center and OWC

The distance between float center and OWC (D/h) plays an important role in affecting the hydrodynamic interaction between the float and the OWC. Effect of D/h on the maximum power absorption efficiency can be found in Fig. 16. As D/h increases from 0.075 to 0.2 with the step of 0.025, the first peak value of η_{max} -kh curve increases proportionally from 0.48 to 0.88, and its corresponding kh also increases from 1.5 to 5.3. Therefore, for a smaller wave frequency there is a demand to deploy a hybrid WEC with a smaller D/h in order to achieve the maximum power absorption efficiency. Conversely, a hybrid WEC with a larger D/h need be deployed. It has to be noted that the smaller D/h is, the smaller the frequency response bandwidth of the hybrid WEC is.

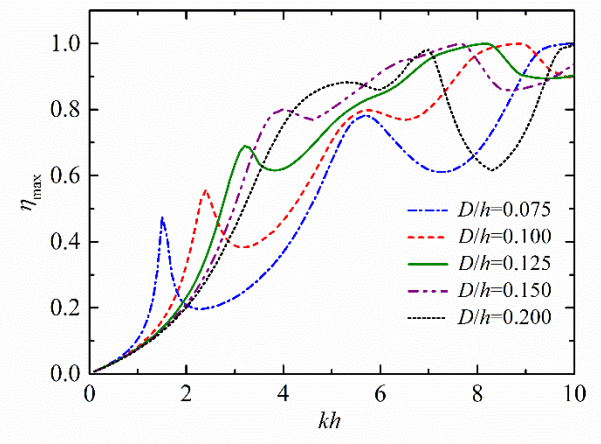

Fig. 16 Variation of η_{max} for various distance between float center and OWC (D/h=0.1) with a_1/h=0.05, a_2/h= a_3/h=0.005, d_1/h=0.05, d_2/h=0.1, d_3/h=0.15, a/h=0.1, d/h=0.1.

4.3.6 Effect of vertical hinge position of the rigid arm

Although the vertical hinge position of the rigid arm (d/h) does not affect the basic hydrodynamic coefficients of the hybrid WEC as calculated in the analytical model, it has a significant influence on the rotary stiffness and inertia of the hinged float. Hence the motion response and power absorption can also be changed by varying d/h, as shown in Fig. 17. As d/h increases from 0.005 to 0.125, the rotary inertia of the float relative to the hinge position increases as well, resulting in a smaller resonant frequency together with a smaller first peak value of $\eta_{\max}$.

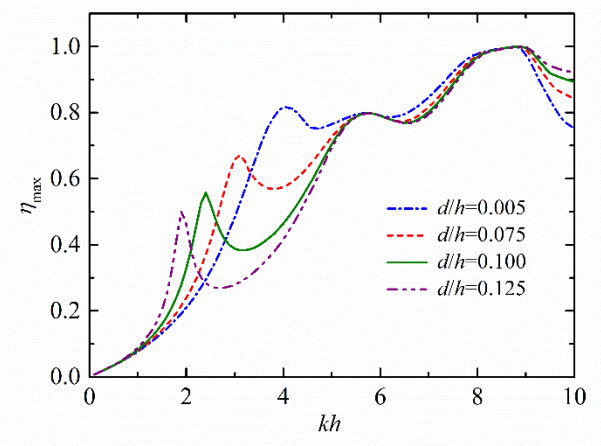

Fig. 17 Variation of $\eta_{\max}$ for various vertical hinge position of the rigid arm (d/h) with a_1/h=0.05, a_2/h= a_3/h=0.005, d_1/h=0.05, d_2/h=0.1, d_3/h=0.15, a/h=0.1, D/h=0.1.

5. Conclusions

We propose a hybrid WEC device consisting of a fixed inverted flume with long length and a bottom hole, and a long floating cube hinged with the flume. An analytical model is developed for the power extraction of the device based on linear potential flow theory and eigen-function matching method in the two-dimensional Cartesian coordinate system.

The wave excitation forces/volume flux, added mass and wave damping are all calculated by the analytical model using different approaches. Additionally, hydrodynamic performance of an OWC consisting of two vertical thin barriers with unequal length is also evaluated and is compared with published results (Falnes and McIver, 1985). The good agreement of these results between each other shows that the present analytical model is correct. In addition, the analytical results of the maximum power absorbed by the device is compared with those using trial-and-error method. Energy conservation relationship is also checked to indirectly validate the present analytical model.

The validated analytical model is then adopted to carry out the study on power capture capability of the device with different geometrical dimension. For some specified dimensions, results are also compared with a parallel study of an isolated OWC and an isolated float. Results reveal that: the power extraction capacity can be significantly improved for a wide range of wave conditions after combining the isolated OWC and the isolated float together. The hydrodynamic interaction

between the float and the OWC plays a positive effect on power absorption of the hybrid WEC for some certain wave conditions.

It is found that the influence of device geometry on the power absorption can be significant and varies considerably, depending on wave length. For $3.0<kh<4.0$, the hybrid WEC with a larger water column width inside the OWC chamber, a larger submergence of the side walls of the OWC chamber, a larger float width, while a smaller float draft is welcome in absorbing more power from incident waves. As *kh* increase from 0 towards 5.0, there is generally a peak value of $\eta_{\max}$-*kh* curve, which turns larger for the hybrid WEC with a larger water column width inside the OWC chamber, a larger submergence of the side walls of the OWC chamber, a larger float width, a larger distance between the float center and the fore wall of OWC, a smaller float draft and a smaller height of the hinge relative to the mean water surface.

The analytical model proposed in this paper can be applied to study the wave attenuation by the floating breakwaters consisting of a float and an OWC. The wave power absorption obtained by using the potential flow theory in this paper may be overestimated without consideration of water viscous effect. Such viscous effect on the hybrid WEC device might be investigated by using physical experiments in the future. The present work concentrates on analysis of the performance of a two-dimensional hybrid WEC. Analytical study on the power extraction of a three-dimensional hybrid WEC will be reported elsewhere.

Acknowledgements

The research was supported by the National Natural Science Foundation of China (51679124, 51479092), China Postdoctoral Science Foundation (Grant No. 2016M601041, 2017T100085) and Tsinghua National Laboratory for Information Science and Technology.

Appendix A. Expression of the generalized excitation forces in terms of the radiated wave's far-field coefficients

Since $\Phi_{\mathrm{R}}^{(L)}$ (L=1, 2, 3) is the spatial velocity potential due to unit amplitude velocity oscillation of the float in mode L, the component in mode L of the generalized normal vector n_L can be written as

$$n_L = \frac{\partial \Phi_{\mathrm{R}}^{(L)}}{\partial n}, \tag{A1}$$

therefore, Eq. (20) can be rewritten as

$$F_{\mathrm{e}}^{(L)} = -\mathrm{i}\omega\rho\int_{S_1}\left(\Phi_{\mathrm{I}}+\Phi_{\mathrm{D}}\right)\frac{\partial \Phi_{\mathrm{R}}^{(L)}}{\partial n}\mathrm{d}s = -\mathrm{i}\omega\rho\int_{S_1}\left(\Phi_{\mathrm{I}}\frac{\partial \Phi_{\mathrm{R}}^{(L)}}{\partial n}+\Phi_{\mathrm{D}}\frac{\partial \Phi_{\mathrm{R}}^{(L)}}{\partial n}\right)\mathrm{d}s. \tag{A2}$$

According to Green's theorem (Falnes, 2002), we have

$$\int_{S_1}\left(\Phi_{\mathrm{D}}\frac{\partial\Phi_{\mathrm{R}}^{(L)}}{\partial n}-\Phi_{\mathrm{R}}^{(L)}\frac{\partial\Phi_{\mathrm{D}}}{\partial n}\right)\mathrm{d}s=-\int_{S_{\pm\infty}}\left(\Phi_{\mathrm{D}}\frac{\partial\Phi_{\mathrm{R}}^{(L)}}{\partial n}-\Phi_{\mathrm{R}}^{(L)}\frac{\partial\Phi_{\mathrm{D}}}{\partial n}\right)\mathrm{d}s=0, \tag{A3}$$

where $S_{\pm\infty}$ represents the boundaries at infinite, i.e., $x=\pm\infty$.

Hence, together with employment of the boundary condition of wave diffraction at wetted surface, i.e., $\partial\Phi_{\mathrm{D}}/\partial n=-\partial\Phi_{\mathrm{I}}/\partial n$, we have

$$F_{\mathrm{e}}^{(L)}=-\mathrm{i}\omega\rho\int_{S_1}\left(\Phi_{\mathrm{I}}\frac{\partial\Phi_{\mathrm{R}}^{(L)}}{\partial n}+\Phi_{\mathrm{R}}^{(L)}\frac{\partial\Phi_{\mathrm{D}}}{\partial n}\right)\mathrm{d}s=-\mathrm{i}\omega\rho\int_{S_1}\left(\Phi_{\mathrm{I}}\frac{\partial\Phi_{\mathrm{R}}^{(L)}}{\partial n}-\Phi_{\mathrm{R}}^{(L)}\frac{\partial\Phi_{\mathrm{I}}}{\partial n}\right)\mathrm{d}s, \tag{A4}$$

which is one way of formulating the so-called Haskind relation.

If we reuse Green's theorem, wave excitation forces can be written as

$$F_{\mathrm{e}}^{(L)}=\mathrm{i}\omega\rho\int_{S_{\pm\infty}}\left(\Phi_{\mathrm{I}}\frac{\partial\Phi_{\mathrm{R}}^{(L)}}{\partial n}-\Phi_{\mathrm{R}}^{(L)}\frac{\partial\Phi_{\mathrm{I}}}{\partial n}\right)\mathrm{d}s. \tag{A5}$$

The incident wave potential is generally given as:

$$\Phi_{\mathrm{I}}=-\frac{\mathrm{i}gA\mathrm{e}^{\mathrm{i}kx}}{\omega}\frac{\cosh\left[k\left(z+h\right)\right]}{\cosh\left(kh\right)}=-\frac{\mathrm{i}gA\mathrm{e}^{\mathrm{i}kx}}{\omega}\frac{Z_1\left(z\right)}{Z_1\left(0\right)}. \tag{A6}$$

After inserting Eqs. (11) ,(14) and (A6) into Eq.(A5),

$$\begin{aligned}
F_{\mathrm{e}}^{(L)}&=\mathrm{i}\omega\rho\left[\int_{S_{+\infty}}\left(\Phi_{\mathrm{I}}\frac{\partial\Phi_{\mathrm{R}}^{(L)}}{\partial n}-\Phi_{\mathrm{R}}^{(L)}\frac{\partial\Phi_{\mathrm{I}}}{\partial n}\right)\mathrm{d}s+\int_{S_{-\infty}}\left(\Phi_{\mathrm{I}}\frac{\partial\Phi_{\mathrm{R}}^{(L)}}{\partial n}-\Phi_{\mathrm{R}}^{(L)}\frac{\partial\Phi_{\mathrm{I}}}{\partial n}\right)\mathrm{d}s\right]\\
&=\mathrm{i}\omega\rho\left[\int_{S_{+\infty}}\left(\mathrm{i}k\Phi_{\mathrm{I}}\Phi_{\mathrm{R}}^{(L)}-\mathrm{i}k\Phi_{\mathrm{R}}^{(L)}\Phi_{\mathrm{I}}\right)\mathrm{d}s+\int_{S_{-\infty}}\left(-\mathrm{i}k\Phi_{\mathrm{I}}\Phi_{\mathrm{R}}^{(L)}-\mathrm{i}k\Phi_{\mathrm{R}}^{(L)}\Phi_{\mathrm{I}}\right)\mathrm{d}s\right]\\
&=\mathrm{i}\omega\rho\left(-2\mathrm{i}k\right)\int_{-h}^{0}\left[\left(-\frac{\mathrm{i}gA\mathrm{e}^{\mathrm{i}kx}}{\omega}\frac{Z_1\left(z\right)}{Z_1\left(0\right)}\right)\left(A_{1,1}^{(L)}\mathrm{e}^{-\mathrm{i}kx}Z_1\left(z\right)\right)\right]_{x=-\infty}\mathrm{d}z\\
&=\frac{-2\mathrm{i}\rho gAkhA_{1,1}^{(L)}}{Z_1\left(0\right)}
\end{aligned}. \tag{A7}$$

For the excitation volume flux $F_{\mathrm{e}}^{(4)}$, using the free surface boundary conditions of incident and diffracted potentials, its expression as given in Eq. (21) can be written as:

$$F_{\mathrm{e}}^{(4)}=\int_{x_{\mathrm{R},2}}^{x_{\mathrm{L},3}}\frac{\partial\left(\Phi_{\mathrm{I}}+\Phi_{\mathrm{D}}\right)}{\partial z}\Big|_{z=0}\mathrm{d}x=-\mathrm{i}\omega\rho\int_{x_{\mathrm{R},2}}^{x_{\mathrm{L},3}}\left(\Phi_{\mathrm{I}}+\Phi_{\mathrm{D}}\right)\frac{\mathrm{i}\omega}{\rho g}\Big|_{z=0}\mathrm{d}x. \tag{A8}$$

With the employment of the free surface boundary condition of $\Phi_{\mathrm{R}}^{(4)}$ inside the OWC chamber, i.e., Eq. (2), and Green's theorem to Φ_{D} and $\Phi_{\mathrm{R}}^{(4)}$ in a similar way as given in Eq. (A3), we have

$$\begin{aligned} F_{\mathrm{e}}^{(4)} &= -\mathrm{i}\omega\rho\int_{x_{\mathrm{R},2}}^{x_{\mathrm{L},3}}\left(\Phi_{\mathrm{I}}+\Phi_{\mathrm{D}}\right)\left(\frac{\partial\Phi_{\mathrm{R}}^{(4)}}{\partial z}-\frac{\omega^2}{g}\Phi_{\mathrm{R}}^{(4)}\right)\Bigg|_{z=0}\mathrm{d}x \\ &= -\mathrm{i}\omega\rho\int_{x_{\mathrm{R},2}}^{x_{\mathrm{L},3}}\left(\Phi_{\mathrm{I}}\frac{\partial\Phi_{\mathrm{R}}^{(4)}}{\partial z}-\Phi_{\mathrm{R}}^{(4)}\frac{\partial\Phi_{\mathrm{I}}}{\partial z}\right)\Bigg|_{z=0}\mathrm{d}x \end{aligned} \quad . \tag{A9}$$

For the unit normal at either water surface or wetted surface of structures in this paper is defined pointing into the fluid region, thus for the mean water level inside the chamber, $\partial/\partial z=-\partial/\partial n$. Using $\partial/\partial z=-\partial/\partial n$ at the mean water level and applying Green's theorem to Φ_{I} and $\Phi_{\mathrm{R}}^{(4)}$, we have

$$\begin{aligned} F_{\mathrm{e}}^{(4)} &= \mathrm{i}\omega\rho\int_{x_{\mathrm{R},2}}^{x_{\mathrm{L},3}}\left(\Phi_{\mathrm{I}}\frac{\partial\Phi_{\mathrm{R}}^{(4)}}{\partial n}-\Phi_{\mathrm{R}}^{(4)}\frac{\partial\Phi_{\mathrm{I}}}{\partial n}\right)\Bigg|_{z=0}\mathrm{d}x=-\mathrm{i}\omega\rho\int_{S_{\pm\infty}}\left(\Phi_{\mathrm{I}}\frac{\partial\Phi_{\mathrm{R}}^{(4)}}{\partial n}-\Phi_{\mathrm{R}}^{(4)}\frac{\partial\Phi_{\mathrm{I}}}{\partial n}\right)\mathrm{d}s \\ &= -\mathrm{i}\omega\rho\left(-2\mathrm{i}k\right)\int_{-h}^{0}\left[\left(-\frac{\mathrm{i}gA\mathrm{e}^{\mathrm{i}kx}}{\omega}\frac{Z_1(z)}{Z_1(0)}\right)\left(A_{1,1}^{(4)}\mathrm{e}^{-\mathrm{i}kx}Z_1(z)\right)\right]\Bigg|_{x=-\infty}\mathrm{d}z \\ &= \frac{2\mathrm{i}\rho gAkhA_{1,1}^{(4)}}{Z_1(0)} \end{aligned} \quad .\tag{A10}$$

References

Boccotti, P., 2007. Caisson breakwaters embodying and OWC with a small opening- Part I: Theory. Ocean Engineering. 34, 806-819.

Chen, T., Wu, B., Li, M., 2017. Flume experiment study on capture width ratio of a new backward bent duct buoy with a pentagon buoyancy cabin. Ocean Engineering. 141, 12-17.

Deng, Z.Z., Huang, Z.H., Law, A.W.K., 2014. Wave power extraction from a bottom-mounted oscillating water column converter with a V-shaped channel. Proceedings of the Royal Society A. 470: 20140074.

Elhanafi, A., Fleming, A., Macfarlane, G., et al., 2016. Numerical energy balance analysis for an onshore oscillating water column-wave energy converter. Energy. 116 (Part 1), 539-557.

Elhanafi, A., Fleming, A., Macfarlane, G., et al., 2017. Underwater geometrical impact on the hydrodynamic performance of an offshore oscillating water column-wave energy converter. Renewable Energy. 105, 209-231.

Evans, D.V., 1982. Wave-power absorption by systems of oscillating surface pressure distributions. Journal of Fluid Mechanics. 114, 481-499.

Evans, D.V., Porter, R., 1995. Hydrodynamic characteristics of an oscillating water column device. Applied Ocean Research. 17, 155-164.

Falnes, J., 2002. Ocean waves and oscillating systems- linear interactions including wave-energy extraction. Cambridge: Cambridge University Press.

Falnes, J., McIver, P, 1985. Surface wave interactions with system of oscillating bodies and pressure distributions. Applied Ocean Research. 7(4), 225-234.

He, F., Huang, Z., 2017. Characteristics of orifices for modelling nonlinear power take-off in wave-flume tests of oscillating water column devices. Journal of Zhejiang University-Science A. 18(5), 329-345.

He, F., Huang, Z., Law, A.W.K., 2013. An experimental study of a floating breakwater with asymmetric pneumatic chambers for wave energy extraction. Applied Energy. 106, 222-231.

He, F., Leng, J., Zhao, X., 2017. An experimental investigation into the wave power extractions of a floating box-type breakwater with dual pneumatic chambers. Applied Ocean Research. 67, 21-30.

Heath, T.V., 2012. A review of oscillating water columns. Philosophical Transactions of the Royal Society A. 370, 235-245.

Iturrioz, A., Guanche, R., Lara, J.L., et al., 2015. Validation of OpenFOAM for oscillating water column three-dimensional modeling. Ocean Engineering. 107, 222-236.

López, I., Pereiras, B., Castro, F., et al., 2014. Optimisation of turbine-induced damping for an OWC wave energy converter using a RANS-VOF numerical model. Applied Energy. 127, 105-114.

López, I., Pereiras, B., Castro, F., et al., 2016. Holistic performance analysis and turbine-induced damping for an OWC wave energy converter. Renewable Energy. 85, 1155-1163.

Malara, G., Arena, G., 2013. Analytical modelling of an U-Oscillating Water Column and performance in random waves. Renewable Energy. 60, 116-126.

Morris-Thomas, M. T., Irvin, R.J., Thiagarajan, K. P., 2007. An investigation into the hydrodynamic efficiency of an oscillating water column. Journal of Offshore Mechanics and Arctic Engineering. 129(4), 273-278.

Ning, D., Wang, R., Zhang, C., 2017. Numerical simulation of a dual-chamber oscillating water column wave energy converter. Sustainability. 9, 1599. doi:10.3390/su9091599

Ning, D.Z., Shi, J., Zou, Q.P., et al., 2015. Investigation of hydrodynamic performance of an OWC (oscillating water column) wave energy device using a fully nonlinear HOBEM (higher-order boundary element method). Energy. 83, 177-188.

Noad, I., Porter, R., 2017. Wave energy absorption by a shallow-draughted rectangular barge of oscillating water columns. Proceedings of the 12th European Wave and Tidal Energy Conference. 27th Aug-1st Sept, 2017, Cork, Ireland. 651, pp. 1-9.

Rezanejad, K., Bhattacharjee, J., Guedes Soares, C., 2013, Analytical and numerical study of nearshore multiple oscillating water columns. Proceedings of the ASME 2013 32ND International Conference on Ocean, Offshore and Arctic Engineering. June 9-14, 2013, Nantes, France. pp. 1-8.

Rezanejad, K., Bhattacharjee, J., Guedes Soares, C., 2015, Analytical and numerical study of dual-chamber oscillating water columns on stepped bottom. Renewable Energy. 75, 272-282.

Sarmento, A.J.N.A., 1992. Wave flume experiments on two-dimensional oscillating water column wave energy devices. Experiments in Fluids. 12, 286-292.Sheng, W, Alcorn, R., Lewis, A., 2014. Assessment of primary energy conversions of oscillating water columns. I.

Hydrodynamic analysis. Journal of Renewable and Sustainable Energy. 6,053113(2014); DOI: 10.1063/1.4896850.

Sarmento, A.J.N.A., Falcão, A.F.O., 1985. Wave generation by an oscillating surface-pressure and its application in wave-energy extraction. Journal of Fluid Mechanics. 150, 467-485.

Zhang, Y., Zou, Q.P., Greaves, D., 2012. Air-water two-phase flow modelling of hydrodynamic performance of an oscillating water column device. Renewable Energy. 41, 159-170.

Zheng, S., and Zhang, Y., 2016. Wave diffraction and radiation by multiple rectangular floaters. Journal of Hydraulic Research. 54:1, 102-115.

Zheng, Y.H., You, Y.G., Shen, Y.M., 2004. On the radiation and diffraction of water waves by a rectangular buoy. Ocean Engineering. 31, 1063-1082.